



# Capillary Pressure in Unsaturated Food Systems: Its Importance and Accounting for It in Mathematical Models

Yash Shah<sup>1</sup> · Pawan Singh Takhar<sup>1</sup>

Received: 28 February 2023 / Accepted: 4 March 2023 / Published online: 21 March 2023  
© The Author(s), under exclusive licence to Springer Science+Business Media, LLC, part of Springer Nature 2023

## Abstract

Capillary pressure plays a critical role in driving fluid flow in unsaturated porous (pores not saturated with liquids but also containing air/gas) structures. The role and importance of capillary pressure have been well documented in geological and soil sciences but remain largely unexplored in the food literature. Available mathematical models for unsaturated food systems have either ignored the capillary-driven flow or combined it with the diffusive flow. Such approaches are bound to impact the accuracy of models. The derivation of the microscale definition of capillary pressure is overviewed, and the limitations of using the microscale definition at the macroscale are discussed. Next, the factors affecting capillary pressure are briefly reviewed. The parametric expressions for capillary pressure as a function of saturation and temperature, developed originally for soils, are listed, and their application for food systems is encouraged. Capillary pressure estimation methods used for food systems are then discussed. Next, the different mathematical formulations for food systems are compared, and the limitations of each formulation are discussed. Additionally, examples of hybrid mixture theory-based multiscale models for frying involving capillary pressure are provided. Capillary-driven liquid flow plays an important role in the unsaturated transport during the processing of porous solid foods. However, measuring capillary pressure in food systems is challenging because of the soft nature of foods. As a result, there is a lack of available capillary pressure data for food systems which has hampered the development of mechanistic models. Nevertheless, providing a fundamental understanding of capillary pressure will aid food engineers in designing new experimental studies and developing mechanistic models for unsaturated processes.

**Keywords** Unsaturated · Porous · Capillary · Pressure · Saturation · Modeling

## Nomenclature

### Latin symbols

$A$	Pre-exponential factor (Eq. (43)) $\left(\frac{\text{m}^2}{\text{s}}\right)$
$a$	Constant in the linear relation between $\gamma^{wn}$ and $T$ (Eq. (22)) (N/m)
$a_s$	Radius of sphere (Eq. (42)) (m)
$a_w$	Water activity (Eq. (39)) (dimensionless)
$a_0^{ws}$	Coefficient in the power series expression for the interfacial energy per unit area (Eq. (28)) $\left(\frac{\text{N}}{\text{m}}\right)$

$a_0^{ns}$	Coefficient in the power series expression for the interfacial energy per unit area (Eq. (29)) $\left(\frac{\text{N}}{\text{m}}\right)$
$a_1^{ws}$	Coefficient in the power series expression for the interfacial energy per unit area (Eq. (28)) $\left(\frac{\text{N}}{\text{mK}}\right)$
$a_1^{ns}$	Coefficient in the power series expression for the interfacial energy per unit area (Eq. (29)) $\left(\frac{\text{N}}{\text{mK}}\right)$
$B$	Mixture viscosity of the biopolymeric matrix (Eq. (48)) (Pa.s)
$b$	Constant in the linear relation between $\gamma^{wn}$ and $T$ (Eq. (22)) $\left(\frac{\text{N}}{\text{mK}}\right)$
$C$	Liquid concentration (Eq. (40)) (amount of substance)
$C_0$	Constant surface concentration (Eq. (42)) (amount of substance)
$C_1$	Initial uniform concentration (Eq. (42)) (amount of substance)
$c^l$	Mass concentration of liquid (Eq. (45)) $\left(\frac{\text{kg}}{\text{m}^3}\right)$
$c^{ws}$	Constant (Eq. (30)) $\left(\frac{\text{N}}{\text{mK}}\right)$

Corresponding author has been previously published as Pawan P. Singh.

✉ Pawan Singh Takhar  
ptakhar@illinois.edu

<sup>1</sup> Department of Food Science and Human Nutrition, University of Illinois at Urbana-Champaign, Urbana, IL 61801, USA

$c^{ns}$	Constant (Eq. (31)) $\left(\frac{N}{mK}\right)$	$r$	Capillary radius (m)
$C_p^\alpha$	Specific heat for phase $\alpha$ (Eq. (52)) $\left(\frac{J}{kgK}\right)$	$r$	Radial distance (m)
$D_{eff}$	Effective diffusivity (Eq. (43)) $\left(\frac{m^2}{s}\right)$	$S_w$	Wetting phase saturation (dimensionless)
$D^\alpha$	Diffusivity of phase $\alpha$ (Eq. (48)) $\left(\frac{m^2}{s}\right)$	$S_e$	Effective saturation of the wetting phase (dimensionless)
$D_c$	Concentration gradient dependent capillary diffusivity (Eq. (46)) $\left(\frac{m^2}{s}\right)$	$S_s$	Saturated wetting phase saturation (dimensionless)
$D_w$	Capillary diffusivity of water (Eq. (47)) $\left(\frac{m^2}{s}\right)$	$S_r$	Residual wetting phase saturation (dimensionless)
$D_T$	Temperature gradient dependent capillary diffusivity (Eq. (46)) $\left(\frac{m^2}{s}\right)$	$S^{\alpha\beta}$	Interface stress tensor (Eq. (1)) $\left(\frac{N}{m}\right)$
$E_a$	Activation energy (Eq. (43)) $\left(\frac{J}{mol}\right)$	$s$	Distance (Eq. (44)) (m)
$E$	Modulus of elasticity of the biopolymeric matrix (Eq. (48)) (Pa)	$T_a$	Stress tensor for adjacent phases (Eq. (1)) $\left(\frac{N}{m^2}\right)$
$\beta\hat{e}^\alpha$	Source-sink term (Eq. (49)) $\left(\frac{kg}{m^3s}\right)$	$T$	Temperature (K)
$F$	Resultant of the elastic surface forces acting on the contact line (Eq. (5)) (N/m)	$T_r$	Reference temperature (K)
$g$	Gravitational acceleration (m/s <sup>2</sup> )	$T_f$	Target temperature (K)
$h$	Capillary pressure head (m)	$U$	Velocity of the interface (Eq. (1)) $\left(\frac{m}{s}\right)$
$h_b$	Bubbling pressure head (Eq. (1)9) (m)	$u^{s,\alpha\beta}$	Interfacial energy per unit area for an interface formed by phase $\alpha$ and $\beta$ (Eq. (27)) $\left(\frac{J}{m^2}\right)$
$\Delta_{sn}^{sw}h^s$	Enthalpy of immersion per unit area (Eq. (21)) (J/m <sup>2</sup> )	$v^{\alpha,s}$	Velocity of $\alpha$ phase with respect to the solid phase (Eq. (48)) $\left(\frac{m}{s}\right)$
$I$	Identity tensor (Eq. (3)) (dimensionless)	$v_{\alpha\beta}$	Normal to the contact line (Eq. (5)) (dimensionless)
$I^\sigma$	$I - NN$ , Projected surficial identity tensor (Eq. (2)) (dimensionless)	$v_w$	Molar volume of water (Eq. (39)) (m <sup>3</sup> mol <sup>-1</sup> )
$j_m$	Mass flux of liquid phase (Eq. (44)) $\left(\frac{kg}{m^2s}\right)$	$v$	Velocity of adjacent phases at the interface (Eq. (1)) $\left(\frac{m}{s}\right)$
$K^\alpha$	Permeability of phase $\alpha$ (Eq. (48)) (m <sup>2</sup> )	<b>Greek symbols</b>	
$k^\alpha$	Thermal conductivity of phase $\alpha$ (Eq. (52)) $\left(\frac{W}{mK}\right)$	$\Gamma$	Excess mass of the interface (Eq. (1)) $\left(\frac{kg}{m^2}\right)$
$k$	Restriction on fitting parameters of van Genuchten's function (Eq. (17)) (dimensionless)	$\rho$	Density $\left(\frac{kg}{m^3}\right)$
$M$	Moisture content on a dry basis (Eq. (47)) $\left(\frac{g}{gsolids}\right)$	$\rho_l$	Liquid density (Eq. (37)) $\left(\frac{kg}{m^3}\right)$
$M_w$	Molecular weight (Eq. (37)) $\left(\frac{kg}{mol}\right)$	$\rho^\alpha$	Density of phase $\alpha$ (Eq. (49)) $\left(\frac{kg}{m^3}\right)$
$m$	Fitting parameter for van Genuchten's function (Eq. (15)) (dimensionless)	$\gamma$	Interfacial tension $\left(\frac{N}{m}\right)$
$N$	Unit vector normal to the interface (towards $\alpha$ phase) (Eq. (1)) (dimensionless)	$\gamma^{wn}$	Interfacial tension between $w$ and $n$ (Eq. (2)) $\left(\frac{N}{m}\right)$
$n$	Fitting parameter for van Genuchten's function (Eq. (15)) (dimensionless)	$\Lambda$	Unit vector tangent to the contact line (Eq. (5)) (dimensionless)
$p^\alpha$	Pressure of phase $\alpha$ (Eq. (45)) $\left(\frac{N}{m^2}\right)$	$\tau^{wn}$	Viscous stress tensor for $wn$ interface (Eq. (2)) $\left(\frac{N}{m}\right)$
$p^c$	Microscale capillary pressure (Pa)	$\tau^\alpha$	Viscous stress tensor for phase $\alpha$ (Eq. (3)) $\left(\frac{N}{m^2}\right)$
$P^c$	Macroscopic capillary pressure (Pa)	$\gamma^{wns}$	Contact curve compression (Eq. (5)) (N)
$P$	Vapor pressure over the meniscus (Eq. (37)) (Pa)	$\theta$	Contact angle (°)
$P_0$	Vapor pressure over the planar surface (Eq. (37)) (Pa)	$\lambda$	Fitting parameter for Brooks and Corey's expression (Eq. (18)) (dimensionless)
$P^b$	Bubbling pressure (Eq. (18)) (Pa)	$\lambda_v$	Latent heat of vaporization (Eq. (52)) $\left(\frac{J}{kg}\right)$
$R$	Universal gas constant $\left(\frac{J}{molK}\right)$	$\alpha$	Fitting parameter for van Genuchten's function (Eq. (15)) $\left(\frac{1}{m}\right)$
$R_c$	Radius of curvature of the liquid surface in the tube (Eq. (37)) (m)	$\beta_0$	Parameter in $p^c(T)$ expression (Eq. (33))
		$\beta_1$	Parameter in $p^c(T)$ expression (Eq. (33))
		$\beta_2$	Parameter in $p^c(T)$ expression (Eq. (33))

$\mu$	Dynamic viscosity (Pa.s)
$\mu^\alpha$	Dynamic viscosity of phase $\alpha$ (Eq. (48)) (Pa.s)
$\beta$	Angle formed by the capillary tube with the vertical direction (Eq. (35))
$\varepsilon^\alpha$	Volume fraction of phase $\alpha$ (Eq. (48)) (dimensionless)
$\dot{\varepsilon}^\alpha$	Material time derivative of volume fraction of phase $\alpha$ with respect to the solid phase (Eq. (48)) ( $s^{-1}$ )
$\phi$	Porosity (Eq. (51)) (dimensionless)

### Superscripts

$\alpha$	General representation for a phase
$\beta$	General representation for a phase
$w$	Wetting phase
$n$	Non-wetting phase
$l$	Liquid
$w$	Water phase
$o$	Oil phase
$g$	Gas phase

### Special symbols

$\frac{D^\sigma}{Dt}$	Surface material derivative (Eq. (1)) (1/s)
$\frac{Dl}{Dl}$	$\nabla^\sigma = \nabla - NN \cdot \nabla$ , Surface gradient operator (Eq. (1)) (1/m)
$\nabla^c$	$\nabla^c = \Lambda \Lambda \cdot \nabla$ , Curvilinear del operator (Eq. (5)) (1/m)
$\langle \rangle$	Averaging operator (Eq. (12)) (dimensionless)
$D^\sigma / Dt$	Material time derivative with respect to the solid phase (Eq. (49)) (1/s)
$[[K]]$	$[[K]] = K^\alpha - K^\beta$ , Jump in the quantity $K$

## Introduction

Capillary action is a key characteristic of all unsaturated porous structures. Soils, rocks, food stuffs, and biological tissues are some common examples of materials involving unsaturated transport. Since the porous structures bearing multiple phases are ubiquitously found in nature, so is the effect of capillary action [1]. This encouraged extensive research in this field, which began nearly two centuries ago with two well-known polymaths, Thomas Young and Pierre-Simon Laplace, as the earliest pioneers. The quest to fully understand and elucidate capillarity continues in various fields, with researchers tackling increasingly challenging problems encountered while studying capillarity. Some of these problems will be introduced in later sections.

Typical examples of capillary action are the rise of water and drop of mercury levels in a thin capillary tube dipped in a bulk of the two fluids, respectively (Fig. 1). An explanation of this phenomenon can be provided in terms of the affinity of a phase towards itself (cohesion) and its affinity towards other phases (adhesion). In the example of an

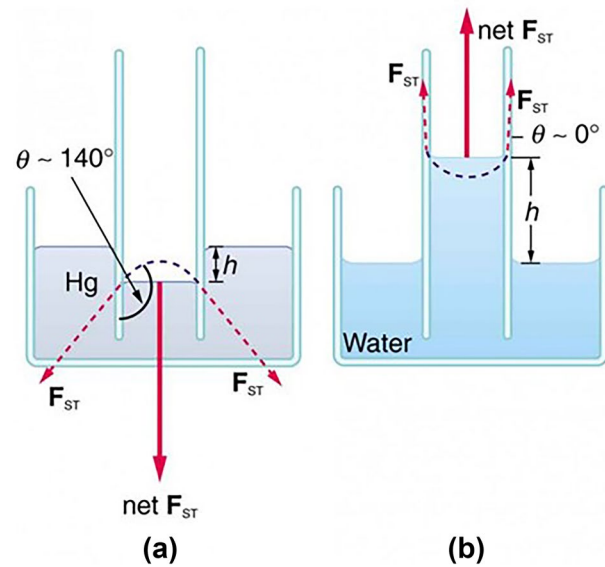


**Fig. 1** Capillary action in vessel filled with **a** mercury, **b** water (reprinted from *Fundamentals of Heat, Light & Sound* [2]). **CC BY 4.0**

air–water–solid system, the higher affinity of the wetting phase (water) for the solid phase (capillary tube) causes the interface to reorient from an initial flat configuration and form a concave meniscus toward air. This meniscus rises in the capillary tube, pulling the wetting phase with it until a new equilibrium position is reached. Conversely, in the air–mercury–solid example, stronger cohesive forces in mercury (non-wetting phase) lead to the development of a convex meniscus that falls in the capillary tube below the level of the bulk fluid.

The driving force for this capillary action is defined as the capillary pressure. Discussions about transport in unsaturated porous structures would hence be incomplete without critically examining the role of capillary pressure.

A more fundamental explanation of this phenomenon can be provided in terms of the interfacial tension and fluid pressures that act on the deformable interface between the immiscible fluids and the collective action of the interfacial tensions acting on the intersection of the three phases known as the common line or contact line. A detailed description and a formal derivation will be provided in “[Capillary Pressure Definition](#).”

## Food as an Unsaturated Porous Medium

Despite important implications, capillary pressure in food systems has not received sufficient attention and rigorous treatment, unlike other fields of study discussed in “[Applications of Capillary Pressure in Other Fields](#).” Before discussing capillary pressure development during

the processing of foods, to get a better intuition, we will describe the porous structure of foods using plant-based foods as an example. A similar deduction can be made for other porous foods by changing the underlying structures. Microstructural features of plant foods play an important role in governing the movement of various phases within the food. Some of these features include the size and orientation of cells, the thickness of cell walls, and the presence of intercellular spaces [3]. These intercellular spaces make up a significant portion of the plant tissue [3], giving the food a porous structure.

The porous structure of plant foods can be characterized as being unsaturated due to the presence of water vapor and carbon dioxide produced from respiration along with liquid water [4]. The level of unsaturation varies from one plant food to another and varies within one plant food depending on environmental and processing conditions. Most foods fall under the category of capillary porous materials with a pore diameter below  $10^{-7}m$ , where capillary pressure-induced forces are crucial to understand transport phenomena [5].

Common food processing operations like conventional drying, microwave drying, extrusion, frying, baking, and reconstitution of dried foods involve capillary pressure development in the porous food matrix. For example, frying in hot oil involves rapid vapor generation and gas expansion within the food matrix [6, 7]. The increase in the gas phase (non-wetting) fraction in the pores leads to the development of capillary pressure in the food matrix. The capillary pressure is expected to increase as more water is lost from the food system. Consequently, the capillary pressure has an increasing impact on further water movement. Similarly, water imbibition during the rehydration of dried foods is driven by capillary forces Weerts et al. [8]. As a result, any attempt to fundamentally understand and predict the outcomes of these processes would be seriously hampered without carefully accounting for capillary pressure-driven transport.

That said, the scarce availability of capillary pressure data in the context of food systems has posed challenges for physics-based modeling approaches. Some studies have relied on empirical expressions from other fields like wood science and soil science [9–11]. Some studies used certain expressions that lump the effect of capillary pressure with other terms or used effective diffusivity-based expressions [12–14]. Any of these approaches are bound to have a negative impact on the model accuracy while also giving them an empirical nature [15]. This also complicates comparing different mathematical models while limiting a given model's adaptability to different products. Lack of information on capillary pressure has also limited mechanistic understanding of processes such as frying, high-temperature baking, microwave heating, expansion of extrudate, etc., where vapor or gas phases are involved.

## Applications of Capillary Pressure in Other Fields

The consequences of capillary pressure development are crucial to many industries and fields of study. One such example is the oil and gas industry, which aims to increase production flow rates to meet rising energy demands. Geophysicists, reservoir engineers, and other petroleum engineers make significant use of the knowledge of capillary pressure for evaluating reservoir quality, expected fluid saturations, seal capacity, depths of fluid contact, and recovery efficiency [16]. The capillary pressure also helps to estimate the thickness of the transition zone, a region with vast amounts of recoverable oil [17].

The study of soils also relies on capillary pressure to explain various observations. For example, water under the influence of gravitational pull alone would settle into the water table, where it saturates the soil leaving the upper layers of soil completely dry. However, we observe regions of unsaturation or partial saturation in the soil above the water table owing to capillary pressure-driven upward water movement [18]. The elevation of water above the water table is expected to be higher in finer soils with smaller pores and channels as compared to coarser soils [19].

Irrigation scheduling is crucial to achieving good crop yields by maintaining optimum water levels in the soil. One widely used soil moisture-based approach for irrigation scheduling involves measuring the soil matric potential (SMP) using a tensiometer [20]. The SMP is a manifestation of the capillary pressure and is described as the force with which water is held in the solid matrix, generally expressed in *kPa*. The threshold matric potential above which irrigation must be done to avoid increasingly poor yields varies from one crop to another [21].

Plant hydraulics is another field of study dealing with capillary pressure. Plants lose a significant amount of water through transpiration, which needs to be replaced by water uptake from the soil. The elongated tubes formed by xylem cells in vascular plants provide the channels for fluid flow. This is a passive transport mechanism requiring no use of the plant's energy, hence preserving the energy for metabolic activities [22].

## Objectives of the Review

The primary motivation for this paper is to provide a mechanistic understanding of capillary pressure in the context of food systems. A detailed discussion on capillary pressure is missing in the food literature. The importance of capillary pressure and its related applications have received attention in soil, wood, and geological sciences for many decades. This can also be inferred from the year of publication of some of the studies cited in this paper. Capillary pressure research in these fields has moved to studying more

complicated phenomena like hysteresis and the dynamic nature of the capillary flow. Regarding food systems, little availability of capillary pressure data combined with an incomplete mechanistic understanding means that there are potential knowledge gaps in the existing food literature. While it is encouraged that new experimental studies are carried out, measuring capillary pressure for food systems is certainly not easy (discussed in “Capillary Pressure Measurement in Foods”) and may require large collaborative efforts. By bringing the capillary pressure discussion to food systems, this study aims to help food researchers build a fundamental understanding of capillary pressure and explicitly outline the assumptions made in some commonly used capillary pressure models. The former saves time and effort for food engineers looking to build mechanistic models involving capillary pressure. The latter creates awareness about certain simplifying assumptions that limit the validity of some commonly employed models, which may or may not be stated clearly elsewhere.

The specific objectives of this review include (1) providing an overview of the microscale derivation of capillary pressure and its upscaled version at the macroscale, (2) discussing the factors affecting capillary pressure, (3) listing some available saturation and temperature-dependent parametric expressions for capillary pressure, (4) reviewing capillary pressure estimation methods used for foods, (5) presenting various mathematical models developed for unsaturated food systems, and (6) reviewing hybrid mixture theory (HMT)–based models for frying.

### Capillary Pressure Definition

The motivation to define capillary pressure comes from the lack of understanding or, rather, misinterpretation of commonly used expressions in the literature [23]. Capillary pressure is generally defined as the difference in pressure between the non-wetting and wetting phases. This definition of capillary pressure has three notable limitations. First, it expresses the capillary pressure as a function of fluid pressures, which are not intrinsic properties of the interface. Second, this definition was developed at the microscale but has been used ubiquitously at the macroscale. Third, it is valid

only at equilibrium but has been used for dynamic situations in the literature. Therefore, it is essential to fully understand the assumptions involved in this definition by reviewing the derivation of capillary pressure at the microscale.

### Microscale Definition

At the microscale, the presence of a wetting and a non-wetting phase in a capillary channel leads to the development of an interface between the two phases and the formation of a contact line where all three phases (wetting, non-wetting, and solid) intersect (Fig. 2). The net force on the fluid–fluid interface is a result of the forces exerted by the fluids on the interface and forces within the interface. The interaction between the solid–fluid and fluid–fluid interfaces dictates the contact line movement. The forces present at the interface and the contact line are best represented by momentum balance equations over the two entities. The momentum balance equation for an interface between phases  $\alpha$  and  $\beta$  is given by [24],

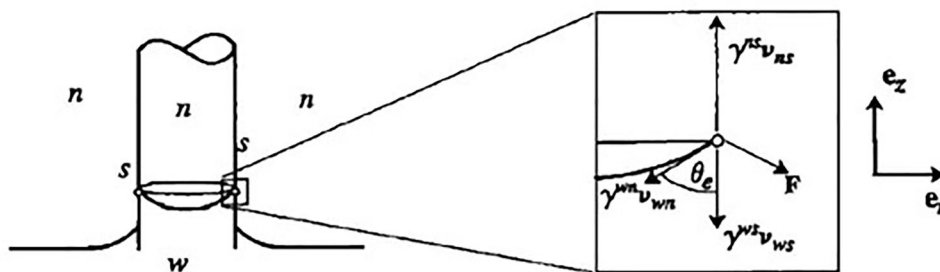
$$\Gamma \frac{D^\sigma U}{Dt} - \Gamma g - \nabla^\sigma \cdot S^{\alpha\beta} + N \cdot [[\rho(v - U)(v - U) - T_a]] = 0 \tag{1}$$

where

- $\Gamma$  excess mass of the interface (kg/m<sup>2</sup>)
- $\frac{D^\sigma}{Dt}$  surface material derivative (1/s)
- $U$  velocity of the interface (m/s)
- $g$  gravitational acceleration (m/s<sup>2</sup>)
- $\nabla^\sigma \cdot \nabla^\sigma = \nabla - NN \cdot \nabla$ , surface gradient operator (1/m)
- $S^{\alpha\beta}$  interface stress tensor (N/m)
- $N$  unit vector normal to the interface (towards  $\alpha$  phase) (dimensionless)
- $\rho$  density (kg/m<sup>3</sup>)
- $v$  velocity of adjacent phases at the interface (m/s)
- $T_a$  stress tensor for adjacent phases (N/m<sup>2</sup>)
- $[[K]][[K]] = K^\alpha - K^\beta$ , jump in the quantity  $K$

The first term on LHS of Eq. (1) is the inertial term, the second term is the body force term, the third term is the interfacial stress term, and the last term accounts for momentum transfer to the interface from the adjacent phases. The bulk fluid phases (wetting and non-wetting) and the fluid–fluid interface are assumed to be isotropic and Newtonian. Accordingly, the stress tensors are given by,

**Fig. 2** Force balance at equilibrium (reprinted from Hasanzadeh and Gray [24] with permission from John Wiley and Sons)



$$S^{wn} = \gamma^{wn} I^\sigma + \tau^{wn} \tag{2}$$

$$T_a^\alpha = -p^\alpha I + \tau^\alpha \tag{3}$$

where

- $w$  wetting phase
- $n$  non-wetting phase
- $\gamma^{wn}$  interfacial tension between  $w$  and  $n$  (N/m)
- $I$  identity tensor (dimensionless).
- $I^\sigma$   $I - NN$ , projected surficial identity tensor (dimensionless).
- $\tau^{wn}$  viscous stress tensor for  $wn$  interface (N/m)
- $p^\alpha$  pressure in phase  $\alpha$  (N/m<sup>2</sup>)
- $\tau^\alpha$  viscous stress tensor for phase  $\alpha$  (N/m<sup>2</sup>)

The following assumptions are made to simplify the analysis further: (1) inertial and body force terms are negligible compared to the other terms, (2) mass transfer between surrounding phases and the interface is considered unimportant, (3) viscous effects of the phases interacting with the interface is assumed negligible. Using Eq. (2) and Eq. (3) in Eq. (1) and simplifying based on the assumptions made, we get [24],

$$\nabla^\sigma \gamma^{wn} - N \gamma^{wn} (\nabla^\sigma \cdot N) + \nabla^\sigma \cdot \tau^{wn} - N(p^w - p^n) = 0 \tag{4}$$

The contact line is treated as a one-dimensional continuum at the microscale. An analogous momentum balance equation obtained for the contact line using a similar procedure and assumptions is given by [24],

$$\nabla^c \gamma^{wns} + \gamma^{wns} \nabla^c \Lambda \cdot \Lambda - v_{wn} \gamma^{wn} - v_{ws} \gamma^{ws} - v_{ns} \gamma^{ns} = F \tag{5}$$

where

- $\Lambda$  unit vector tangent to the contact line (dimensionless)
- $\nabla^c \nabla^c = \Lambda \Lambda \cdot \nabla$ , curvilinear del operator (1/m)
- $\gamma^{wns}$  contact curve compression (N)
- $v_{wn}, v_{ws}, v_{ns}$  normals to the contact line (Fig. 2) (dimensionless)
- $F$  resultant of the elastic surface forces acting on the contact line (N/m).

$\gamma^{wns}$  is related to the stress tensor for the contact line, whereas  $F$  accounts for the infinitesimal elastic deformation of the solid–fluid interface.  $F$  may also be treated as a frictional force resisting the movement of the contact line and is, to some extent, responsible for the hysteresis observed in the contact angle.

The normal components of the momentum balance equations are obtained by taking the dot product of Eq. (4) and Eq. (5) with  $N$  and  $e_z$ , respectively. Simplification results in the following momentum balance equations for the fluid–fluid interface and contact line, respectively [24]:

$$-\gamma^{wn} (\nabla^\sigma \cdot N) + (p^n - p^w) = -(\nabla^\sigma \cdot \tau^{wn}) \cdot N \tag{6}$$

$$\gamma^{wn} \cos \theta + \gamma^{ws} - \gamma^{ns} = F \cdot e_z \tag{7}$$

When a thin capillary is dipped in a bulk liquid, the forces acting at the newly formed contact line cause the flat interface to deform into a curved geometry. The curve will be convex or concave depending on the pair of wetting and non-wetting phases. In the case of water and air, we see a concave interface when viewed from the side. The meniscus formation leads to a pressure difference across the interface. This pressure difference drives the movement of the interface till a new equilibrium position is reached. The movement of the interface can be seen as a combination of a change in meniscus curvature and the subsequent movement of the contact line. In fact, it has been shown that when the pressure difference across the interface is changed by a small amount, the curvature of the meniscus reorients to accommodate the small pressure change [24]. However, beyond a certain change in pressure, the contact line will move to find a new equilibrium position. An equilibrium state is reached when the forces acting on the interface and the contact line are balanced. At equilibrium, the momentum balance equations for a spherical meniscus in a circular capillary of radius  $r$  ( $\nabla^\sigma \cdot N = \frac{2 \cos \theta}{r}$ , where  $\theta$  is the contact angle) are given by:

$$(p^n - p^w)_e = \frac{2\gamma^{wn} \cos \theta}{r} \tag{8}$$

$$\gamma^{wn} \cos \theta + \gamma^{ws} - \gamma^{ns} = 0 \tag{9}$$

Here, the viscous contributions,  $\tau^{wn}$ , and the normal component of force on the contact line,  $F \cdot e_z$ , become zero. Equation (9) is known as Young’s equation, whereas Eq. (8) is the Young–Laplace equation.

$$p^c = p^n - p^w \tag{10}$$

$$p^c = \frac{2\gamma^{wn} \cos \theta}{r} \tag{11}$$

The LHS of the Young–Laplace equation is generally defined as the capillary pressure ( $p^c$ ) (Eq. (10)). However, a more accurate definition is given by the RHS, which expresses the capillary pressure as a function of the interfacial properties (Eq. (11)). Young’s equation (Eq. (9)) can be solved to determine the contact angle at natural equilibrium. For other states, a unique value for the contact angle may not exist.

### Macroscale Definition

The macroscale definition for capillary pressure is [25, 23]:

$$P^c = \langle p \rangle^n - \langle p \rangle^w \tag{12}$$

$$P^c = \frac{2\langle\gamma^{wm}\rangle\cos\langle\theta\rangle}{\langle r \rangle} \quad (13)$$

Measuring properties at the microscale is not easy due to the difficulty in devising microscale experiments. This encourages the upscaling of microscale equations to the macroscale. Upscaling involves averaging over a representative elementary volume (REV). Equations (12) and (13) represent the upscaled equations for capillary pressure. The averaging operator is denoted by the angled brackets.  $P^c$  is the macroscopic capillary pressure, whereas  $\langle p \rangle^n$  and  $\langle p \rangle^w$  represent the pressure of the fluid phases averaged over their respective volumes in the REV. However, the microscale equations were defined for the interface and thus can only be surface averaged over that interface. The surface averaged pressures may not be equal to the average over the phase volumes in the REV [24, 26]. As a result, Eqs. (12) and (13) cannot be obtained by a systematic averaging procedure without making further assumptions. Also, it is difficult to define a unique contact angle and capillary radius when we move away from ideal uniform structures to more realistic porous matrices like foods.

It is also important to note that Eqs. (12) and (13) only apply at equilibrium. However, many studies in the literature have used these equations for dynamic situations, which may be a source of potential errors [27]. These errors may be further amplified at the macroscopic scale [26]. Therefore, the widely used macroscopic expressions for capillary pressure (Eqs. (12) and (13)) make approximations, which, though are acceptable, deserve at least a mention noted above.

## Factors Affecting Capillary Pressure

From Eq. (13), we can see that the capillary pressure is dependent on the interfacial tension, contact angle, and pore radius.

### Interfacial Tension and Contact Angle

The interfacial tension between the wetting and non-wetting phase is a function of the intrinsic properties of the two immiscible fluids in contact. Interfacial tension represents the excess energy at the interface due to unsaturated intermolecular interactions, and it tends to minimize the interfacial area [28]. Based on the macroscopic form of the Young–Laplace equation (Eq. (13)), it is expected that the capillary pressure will decrease with a decrease in the interfacial tension. Interfacial tension can be measured using a wide range of techniques summarized and compared in the work of Drelich et al. [28].

Any changes in interfacial tension between the phases will affect the contact angle. Intuitively and also from Eq. (13), it can be inferred that as the contact angle increases,

the capillary pressure decreases. Capillary pressure becomes zero for a flat interface, i.e.,  $\theta_c = 90^\circ$ . The contact angle, which is a measure of wettability, can technically be estimated from Young's equation (Eq. (9)) but experimentally measuring  $\gamma^{ws}$  and  $\gamma^{ns}$  is not very straightforward, and there is not much data available. Furthermore, Young's equation assumes the solid surface to be flat, smooth, non-porous, inert, and homogeneous. For real surfaces, however, metastable states may exist, and consequently, the contact angle may not have a unique value [29]. Contact angle hysteresis is briefly discussed in a subsequent section (“Saturation”). Methods for directly estimating the contact angle are summarized by Alghunaim et al. [30] and Hebbar et al. [29].

Many food formulations include emulsifiers like monoglycerides, diglycerides, esters, and lecithin, which work by reducing the interfacial tension between the immiscible phases. These compounds will hence have an indirect impact on the capillary pressure. Some surface-active compounds may even form during a food process, for example, frying. At high temperatures achieved during frying, the water vapor exiting the food enters the hot oil, causing some hydrolysis reactions [31]. The cleavage of fatty acids from the glycerol backbone produces mono- and diglycerides, which are surface-active in nature. The formation of these compounds is expected to affect the capillary pressure.

### Pore Radius

Apart from the fluid and solid surface properties, the capillary pressure also depends on the pore radius. The inverse proportionality between the two (Eq. (13)) means that thinner capillaries develop higher capillary pressures. This is the reason why water rises higher in thinner capillaries. Food as a porous medium is not a single capillary but rather a bundle of capillaries with a non-uniform pore radius. The capillary pressure at the pore scale hence varies from one pore to another and along the length of a pore. Additionally, during food processing operations like drying, extrusion, or frying, the pores can undergo expansion or contraction along with the food matrix. During processing, the microstructural changes in foods play a critical role in capillary pressure changes. Alam and Takhar [32] studied the microstructural changes during the frying of potato disks using X-ray micro computed tomography. They found that 20s of frying led to a decrease in the number of pores and a compact structure because of starch gelatinization and the subsequent release of biopolymers into the pores (Fig. 3). Their results were consistent with Reeve and Neel [33] and Spiruta and Mackey [34]. With an increase in frying time, they found an increase in pore sizes due to the expansion caused by vapor formation. The larger pores were formed progressively towards the center, starting at the surface (Fig. 4). This is a direct manifestation of the transport phenomenon taking place in the potato disks and is indirectly influenced by the capillary pressure-driven fluid

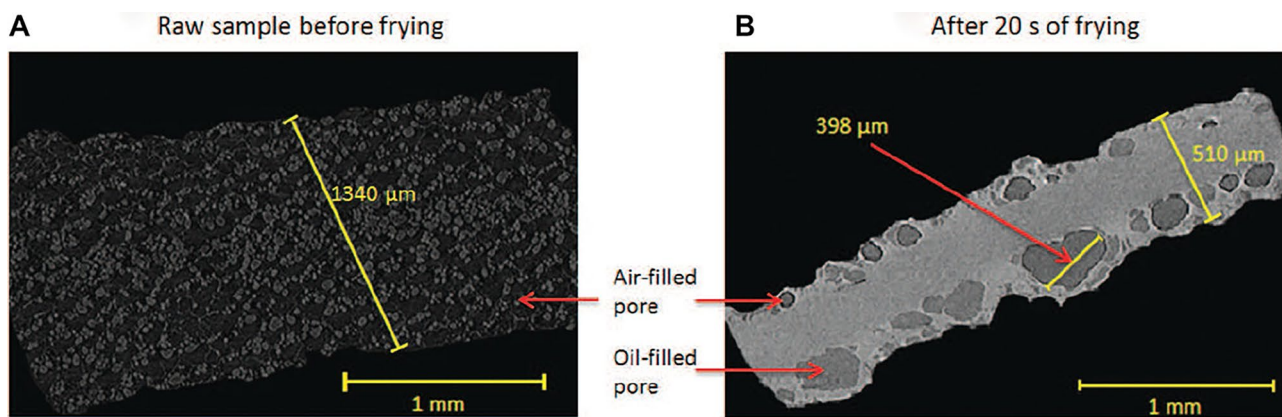


**Fig. 3** X-ray micro-CT images of potato disks **A** before frying, **B** after 20s of frying (reprinted from Alam and Takhar [32] with permission from John Wiley and Sons)

movement. Thus, pore size affects capillary pressure, which, in turn, affects pore size distribution in the food.

### Saturation

In porous materials, the capillary pressure for a given wetting phase is a function of its degree of saturation:

$$P^c = f(S_w) \quad (14)$$

Capillary pressure increases as the wetting phase degree of saturation decreases in the porous matrix [35]. Given the complications involved in measuring the interfacial tension, contact angle, and pore radius, empirical relations expressing capillary pressure as a function of wetting phase saturation have been proposed (Eq. (14)). There are two notable shortcomings when capillary pressure is studied as an explicit function of saturation. The most obvious shortcoming of such an approach is the limited validity to only

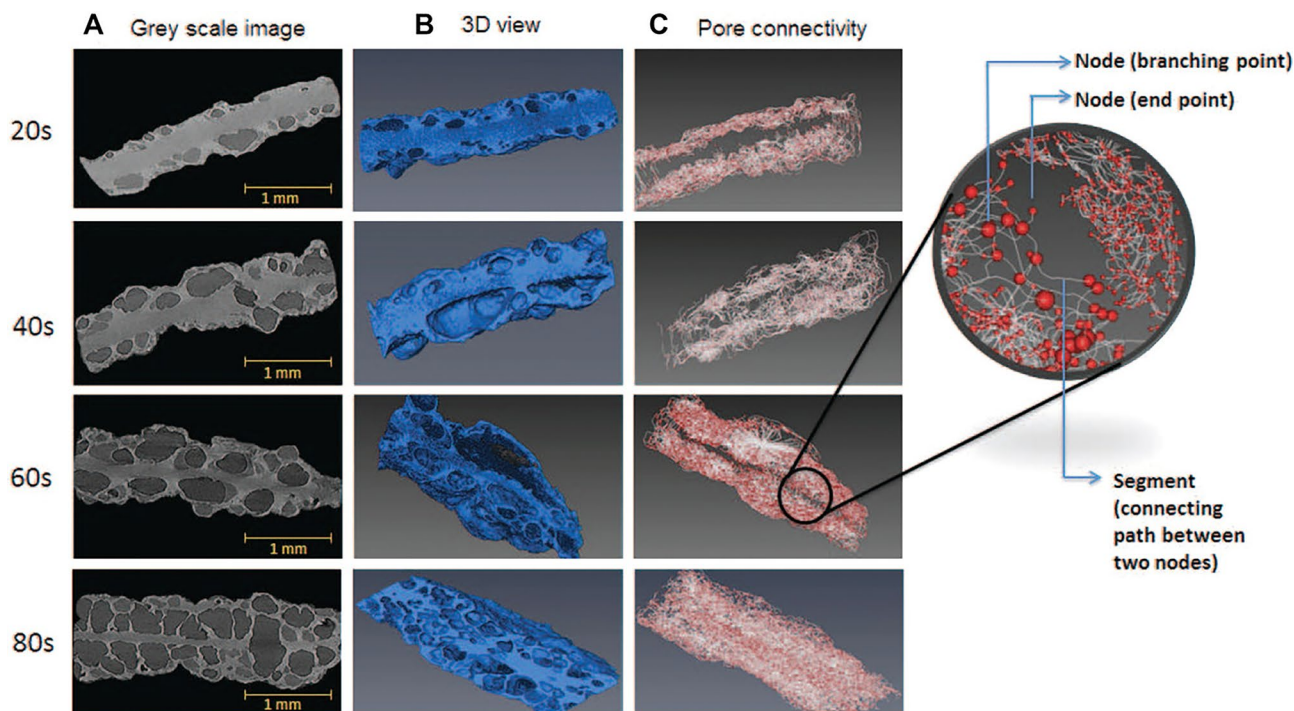


**Fig. 4** **A** X-ray micro-CT images of potato disks after 20, 40, 60, and 80s of frying ( $3.34 \times 3.34 \times 3.34 \mu\text{m}$  voxel size), **B** 3D image of potato disks, **C** pore network model (reprinted from Alam and Takhar [32] with permission from John Wiley and Sons)



the same pair of immiscible fluids, porous structure, and experimental temperature.

The less obvious but significant shortcoming is the non-unique value of capillary pressure at a given saturation. For a given magnitude of capillary pressure, it has generally been observed that the wetting phase saturation is higher during drainage than during wetting experiments [36]. Factors like non-homogeneous pore size distribution, advancing and receding contact angle differences, process-induced structural changes to the porous matrix, air entrapment, and capillary condensation have been hypothesized to be some possible explanations for the observed hysteresis behavior [37]. The presence of hysteresis in capillary pressure measured as a function of saturation has been widely studied in the literature Abbasi et al. [38], Likos et al. [37], Maqsoud et al. [36], Nuth and Laloui [39], Pedroso and Williams [40], Šimůnek et al. [41].

Nevertheless, capillary pressure–saturation functions are widely used firstly because they provide a simple relationship between the macroscale fluid pressures and secondly because their implementation in mathematical models is fairly straightforward [26]. Some available expressions for capillary pressure as a function of wetting phase saturation are discussed in “Capillary Pressure–Saturation Expressions.” The effect of hysteresis on fluid flow is generally neglected as there is a lack of available hysteresis data Šimůnek et al. [41] and accounting for hysteresis complicates the development of mathematical models Abbasi et al. [38].

## Temperature

The effect of temperature on capillary pressure is complex and is of special concern in food processing, where significant temperature changes can occur during a process and temperatures way beyond the boiling point of water may exist. A direct consequence of temperature change is through the change in interfacial tension. Generally, interfacial tension decreases linearly with an increase in temperature [42]. Based on this and as per the Young–Laplace equation (Eq. (13)), capillary pressure is expected to decrease with an increase in temperature. As discussed in “Pore Radius,” high-temperature food processing operations like frying lead to changes in pore size and pore distribution. However, the effect of temperature on pore radius has not been investigated thoroughly. Consequently, some studies assume the pore radius to be independent of the temperature [43].

Some other fields of study, like wood science, assume isothermal or constant temperature conditions, hence ignoring any impact of temperature change on capillary pressure [44, 45]. Such an assumption for food systems would make the mathematical model less rigorous and impact the overall accuracy. However, work done to illustrate the impact of

temperature on capillary pressure in food systems is scarcely available in the literature. It must also be noted that though constant temperature conditions can be assumed for many cases in nature, there might be differences in the temperature at which measurements are made in the lab and the actual real-world temperature, for example, in the reservoir. This has motivated researchers since the mid-1900s to understand the relationship between temperature and capillary pressure. The work of Phillip and de Vries [46] is one such example, although it was found to underestimate the effect of temperature when compared to experimental data [47]. Some expressions available in the literature have been discussed in “Capillary Pressure–Temperature Expressions.”

## Capillary Pressure Parametric Expressions

### Capillary Pressure–Saturation Expressions

A wide range of expressions are available for capillary pressure as a function of wetting phase saturation. Some widely used expressions in the literature are discussed in this section. The expressions are based on the assumption of the nature of the relationship between capillary pressure and saturation expressed as a single or multiparameter explicit function. Consequently, an optimal set of fitting parameters need to be determined using experimental data.

#### Relation of van Genuchten [48]

van Genuchten [48] developed the following empirical relation between wetting phase saturation and capillary head:

$$S_e = \left( \frac{1}{1 + (\alpha h)^n} \right)^m \quad (15)$$

$$h = \frac{1}{\alpha} \left( S_e^{-\frac{1}{m}} - 1 \right)^{\frac{1}{n}} \quad (16)$$

where

$$S_e = \frac{S_w - S_r}{S_s - S_r}$$

Equation (15) [48] is perhaps the most widely used expression that relates the capillary pressure head ( $h$ ) to wetting phase saturation ( $S_w$ ). The capillary pressure head ( $h$ ) can be converted to an equivalent capillary pressure.  $S_e$  is the effective saturation of the wetting phase.  $S_s$  and  $S_r$  represent the saturated and residual wetting phase saturation in the porous medium, respectively.  $\alpha$ ,  $n$ , and  $m$  are the fitting parameters. According to Chen et al. [49],  $\alpha$  is inversely proportional to the non-wetting fluid entry pressure, and  $n$

represents the width of the pore-size distribution. According to Yang and You [50],  $\alpha$  is inversely proportional to the mean pore diameter, and  $n$  and  $m$  are shape parameters. Hence, there are different interpretations of the physical significance of these fitting parameters.

Equation (15) can be rearranged to express the capillary pressure head as an explicit function of saturation (Eq. (16)). Furthermore, many authors prefer to use capillary pressure instead of capillary pressure head, and in such cases, the units of  $\alpha$  will change accordingly [51, 52].

Though the expression was first developed for studying water retention in soils, it can, in principle, be used for all systems, including foods and other biological matrices. This is because a general form of the expression was assumed that did not have a material-specific theoretical basis.

The van Genuchten expression has five undetermined parameters:  $S_s, S_r, \alpha, n,$  and  $m$ . Though all five parameters could technically be optimized to get the best fits, it is advisable to reduce the number of undetermined parameters. This can be done by fixing the value of  $S_s$  and  $S_r$ , or by determining their value through experiments [53]. For example,  $S_s$  can be assumed to be 1, which means that at full saturation, all the pores in the matrix will be filled by the wetting phase. Another approximation that could be made is directly using  $S_w$  instead of  $S_e$  [54].

$$k = m - 1 + \frac{1}{n} \tag{17}$$

van Genuchten [48] used his expression to predict the relative hydraulic conductivity for soil–water systems using Mualem [55] and Burdine’s [56] models. However, in order to get a closed-form expression for conductivity, the values of  $m$  and  $n$  need to be restricted. For Mualem’s [55] model, the restriction is given by Eq. (17), where  $k$  needs to be an integer. For the simplest case of  $k = 0, m = 1 - \frac{1}{n}$ . Though different  $k$  values can be used, there is an increased complexity without significant changes in the results. For Burdine’s [56] model, the restriction on  $m$  and  $n$  is given by  $m = 1 - \frac{2}{n}$ . As a result, the number of undetermined parameters in the expression reduces to 2 ( $\alpha$  and  $n$ ). The fitting of these parameters for different systems has been done extensively in the literature.

Similar efforts need to be undertaken for food systems. Weerts et al. [8] studied the hydration kinetics of dried green tea at different temperatures using a van Genuchten-type water retention curve. Experimentally measured water activity data and the Kelvin equation (Eq. 39, discussed in “Kelvin Capillary Penetration”) were used to determine optimum  $\alpha$  and  $n$  values. The experimental data and fitted van Genuchten model at  $T = 298K$  are shown in Fig. 5.  $\alpha$  and  $n$  values determined for four different temperatures are summarized in Table 1. The magnitude of  $\alpha$  was found to decrease with an increase in temperature, whereas  $n$

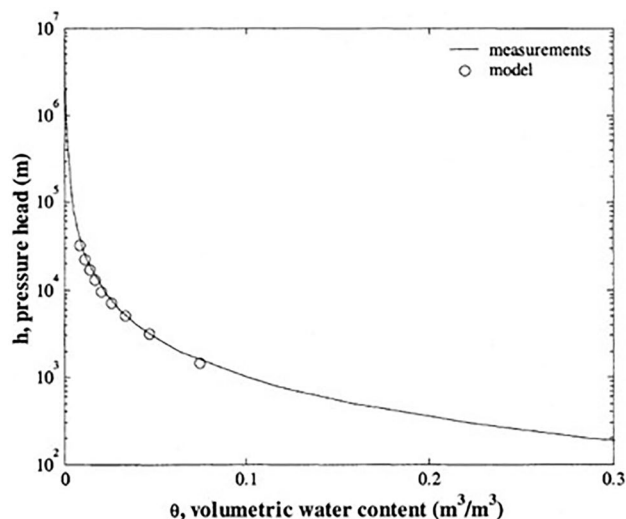


Fig. 5 Fitted van Genuchten expression at  $T = 298K$  for green tea (reprinted from Weerts et al. [8] with permission from John Wiley and Sons)

increased with an increase in temperature. The plots of  $h$  vs  $S_e$  (Eq. (16)) using the values of  $\alpha$  and  $n$  estimated for different temperatures are shown in Fig. 6. Notice the S-shaped nature of the curves. This study is discussed in more detail in “Indirect Measurement.”

**Relation of Brooks and Corey [57]**

Another widely used expression is given by Brooks and Corey [57]:

$$S_e = \left( \frac{P^b}{P^c} \right)^\lambda \text{ for } P^c \geq P^b \tag{18}$$

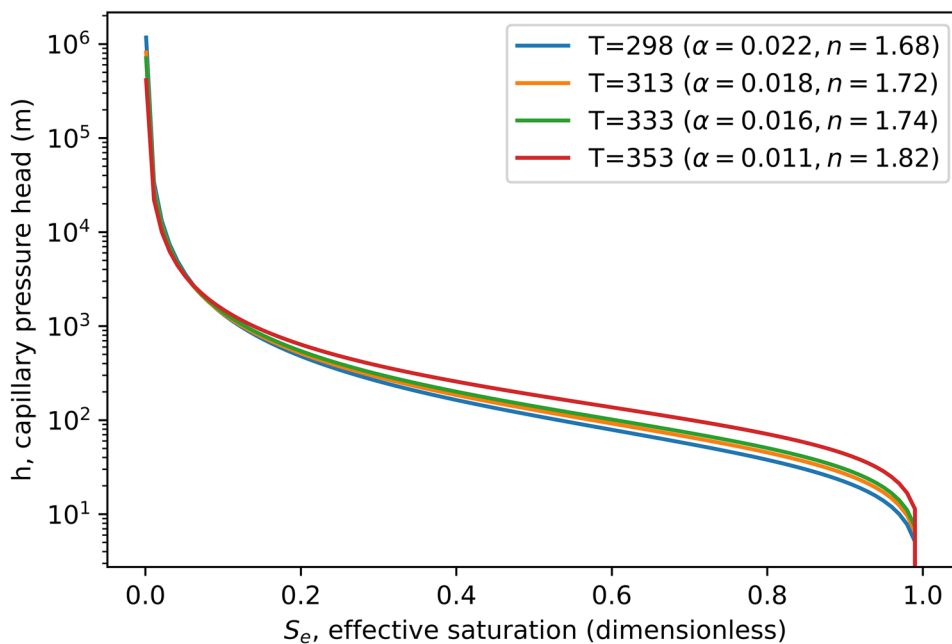
$$S_e = \left( \frac{h_b}{h} \right)^\lambda \tag{19}$$

where  $P^b$  and  $\lambda$  are essentially the fitting parameters and represent the bubbling pressure and pore size distribution index, respectively. The bubbling pressure, which is also referred to in the literature as entry pressure, is defined as the minimum pressure required for the non-wetting phase to

**Table 1** van Genuchten expression parameters at different temperatures for green tea (reprinted from Weerts et al. [8] with permission from John Wiley and Sons)

Temperature (K)	$\alpha$ (m <sup>-1</sup> )	$n$
298	0.022	1.68
313	0.018	1.72
333	0.016	1.74
353	0.011	1.82

**Fig. 6** Plots of capillary pressure head ( $h$ ) vs effective saturation ( $S_e$ ) using the values of  $\alpha$  and  $n$  estimated for green tea at different temperatures by Weerts et al. [8]



enter and displace the wetting phase in a saturated matrix. The range of pore size distribution increases for decreasing  $\lambda$ . Brooks and Corey [57] discuss methods to estimate  $P^b$ ,  $\lambda$ , and  $S_r$ . The expression can also be written in terms of the heads (Eq. (19)) since it's a ratio of pressures. van Genuchten [48] showed that Eq. (15) reduces to Eq. (19) at high values of the capillary pressure head. When a comparison is made between the two expressions, it becomes clear that  $\alpha$  is inversely related to the entry pressure ( $P^b$ ) and  $n$  is the pore size distribution index, as pointed out by Chen et al. [49].

The difference between the S-shaped van Genuchten expression and the convex-shaped Brooks-Corey expression is the representation of the capillary entry pressure [51]. Li et al. [51] showed that (Fig. 7) the Brooks-Corey expression leads to a plateau with a non-zero entry pressure, whereas in van Genuchten's model, the plateau ends with a steep slope that meets the  $x$ -axis at full saturation. Numerous studies have discussed the capillary entry pressure representations, but an agreement on its importance

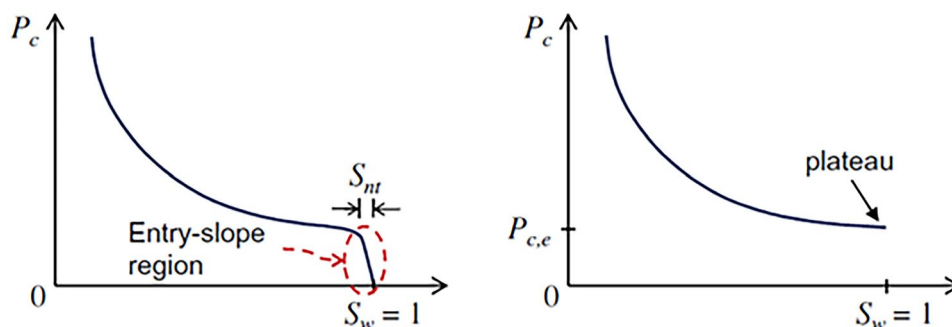
has not been reached. Some convergence and numerical stability issues were found when the van Genuchten expression was used [58]. However, this difference in entry pressure representation does not lead to any significant differences in the capillary pressures estimated away from the endpoint (full saturation).

**Other Expressions**

Many other capillary pressure–saturation expressions have been proposed by Durner [59], Rogers et al. [60], Russo [61], Silin et al. [62], and Webb [52]. However, these expressions were developed for specific systems, and their predictive capabilities have not been tested sufficiently for other systems.

From the above discussion, it can be seen that there are several capillary pressure–saturation expressions available in the literature. Expressions given by van Genuchten [48] and Brooks-Corey (1964) are used more widely than others and are also closely related. Though these were

**Fig. 7** Entry pressure representation for van Genuchten expression (left) and Brooks-Corey expression (right) (reprinted from Li et al. [51] with permission from Elsevier)



proposed for soils and have been used successfully in geological and wood sciences, their generic nature allows us to adopt these expressions for food systems. Experimental data for capillary pressure in food systems can be used for finding the optimum values of the fitting parameters, and the resulting expressions can subsequently be used in mathematical models. However, there is a lack of available capillary pressure data for food systems.

## Capillary Pressure–Temperature Expressions

### Small to Medium Temperature Changes (<20K)

From the Young–Laplace equation (Eq. (13)), we can see that the capillary pressure is expected to change due to the changes in  $\gamma^{wn}$  and  $\cos\theta$  with temperature. Several studies in the literature have shown that a decrease in capillary pressure with an increase in temperature cannot be explained by changes in interfacial tension ( $\gamma^{wn}$ ) alone [63]. Grant and Salehzadeh [43] explored the effect of temperature changes on the wetting coefficient ( $\cos\theta$ ).

Grant and Salehzadeh [43] developed and tested their expression for capillary pressure–temperature relation for two soils (Plano silt loam and Elkmound sandy loam) at several temperatures (5–40 °C), achieving exceptional fits. An overview of the development of their expression is discussed here. It is important to note that the pore radius has been assumed to be independent of temperature and is constant at a given saturation. Furthermore, the wetting coefficient ( $\cos\theta$ ) is a manifestation of changes in  $\gamma^{ns}$  and  $\gamma^{ws}$  with temperature and is independently measurable like  $\gamma^{wn}$  (Eq. (9)).

Taking the temperature derivative of Eq. (11), we get,

$$\frac{\partial p^c}{\partial T} = \frac{p^c}{\gamma^{wn}} \left( \frac{\partial \gamma^{wn}}{\partial T} \right) + \frac{p^c}{\cos\theta} \left( \frac{\partial \cos\theta}{\partial T} \right) \quad (20)$$

All terms on the RHS of Eq. (20) are well studied, and experimental data is available in the literature, with the exception of the  $\frac{\partial \cos\theta}{\partial T}$  term. Using a chemical thermodynamics-based derivation, Grant and Salehzadeh [43] showed that,

$$\frac{d \cos\theta}{dT} = \left( \frac{1}{\gamma^{wn}} \right) \left( \frac{\gamma^{wn} \cos\theta + \frac{\Delta_{sn}^{sw} h^s}{T}}{T} - \cos\theta \frac{d\gamma^{wn}}{dT} \right) \quad (21)$$

where  $\Delta_{sn}^{sw} h^s$  is the enthalpy of immersion per unit area ( $J/m^2$ ). Furthermore, assuming a linear relation between  $\gamma^{wn}$  and temperature,

$$\gamma^{wn} = a + bT \quad (22)$$

where  $a$  and  $b$  are constants, and a temperature-independent value of  $\Delta_{sn}^{sw} h^s$ , it can be shown that the capillary pressure–temperature relationship is of the form,

$$\frac{p^c}{\left( \frac{\partial p^c}{\partial T} \right)} = \beta_0 + T \quad (23)$$

where  $\beta_0$  is a negative constant, and its magnitude depends on  $\Delta_{sn}^{sw} h^s$ , coefficients in the linear relation between  $\gamma^{wn}$  and temperature, and the value of the wetting coefficient at a reference temperature. Finer details about the derivation can be referred to in their work.

$$\frac{p^c}{\left( \frac{\partial p^c}{\partial T} \right)} = \frac{a}{b} + T \quad (24)$$

If the effect of change in wetting coefficient with temperature is ignored, i.e., accounting only for interfacial tension-dependent changes to capillary pressure, an equation (Eq. (24)) similar to Eq. (23) is obtained. The two expressions have the same form and only differ in their intercepts. The intercepts are expected to be an indicator of the relative sensitivity of the capillary pressure to changes in interfacial tension and wetting coefficient.

Integrating Eq. (23) between a reference temperature ( $T_r$ ) and target temperature ( $T_f$ ) leads to the following relation,

$$p_{T=T_f}^c = p_{T=T_r}^c \left( \frac{\beta_0 + T_f}{\beta_0 + T_r} \right) \quad (25)$$

The validity of the above model relies on two assumptions. The first is the linear relationship between  $\gamma^{wn}$  and temperature. There is extensive data available in the literature that supports this assumption for a wide range of fluids and temperature ranges [64, 65, 42]. The second assumption of temperature-independent  $\Delta_{sn}^{sw} h^s$  could be a source of discrepancy. However, despite making these assumptions, Grant and Salehzadeh [43] found a good agreement between experimental and predicted data.  $\beta_0$  was estimated using non-linear regression analysis. For imbibition and drainage data of Plano silt loam,  $\beta_0$  is  $-346.4 K$  and  $-380.4 K$ , respectively. For imbibition data of Elkmound sandy loam,  $\beta_0 = -398.8 K$ . The estimates were made at a reference temperature,  $T_r = 298.15 K$ . The  $\beta_0$  values were estimated using experimental data between 5 and 40 °C, restricting their validity to the same temperature range.

This expression (Eq. (25)) can now be plugged into any of the capillary pressure–saturation expressions discussed in the previous section to get a capillary pressure–saturation–temperature expression. Such expressions can be used in mathematical models, especially for food systems undergoing significant saturation and temperature changes. Experimental studies to estimate the value of  $\beta_0$  for food systems are encouraged.

### Large Temperature Changes (>20K)

$$p^c = \frac{2(\gamma^{ns} - \gamma^{ws})}{r} \tag{26}$$

Grant [66] developed a two-parameter expression for the capillary pressure–temperature relation. Though the two-parameter model, like the one-parameter model, is based on interfacial thermodynamics, it uses Eq. (26) (obtained by combining Eqs. (8) and (9)) as the starting point. The interfacial energy per unit area ( $u^{s,\alpha\beta}$  in J/m<sup>2</sup>) for an interface formed by phase  $\alpha$  and  $\beta$  can be expressed as,

$$u^{s,\alpha\beta} = \gamma^{\alpha\beta} - T \frac{d\gamma^{\alpha\beta}}{dT} \tag{27}$$

A power series expression for the interfacial energy per unit area in terms of temperature was proposed, and the resulting expressions for the wetting phase–solid and non-wetting phase–solid interfacial energies per unit area are given by,

$$u^{s,ws} = \sum_{j=0}^{\infty} a_j^{ws} T^j \tag{28}$$

$$u^{s,ns} = \sum_{j=0}^{\infty} a_j^{ns} T^j \tag{29}$$

where  $a_j^{ws}$  and  $a_j^{ns}$  are coefficients. Using Eqs. (28) and (29) in Eq. (27) and solving the differential equation to find the respective interfacial tensions, we get,

$$\gamma_j^{ws} = a_0^{ws} + a_1^{ws} T \ln T + \sum_{j=2}^{\infty} \frac{a_j^{ws} T^j}{j-1} + c^{ws} T \tag{30}$$

$$\gamma_j^{ns} = a_0^{ns} + a_1^{ns} T \ln T + \sum_{j=2}^{\infty} \frac{a_j^{ns} T^j}{j-1} + c^{ns} T \tag{31}$$

where  $c^{ws}$  and  $c^{ns}$  are constants. Combining Eqs. (26), (30), and (31) gives,

$$p^c = \frac{2}{r} \left[ (a_0^{ns} - a_0^{ws}) + T \ln T [(a_1^{ns} - a_1^{ws})] + T [(c^{ns} - c^{ws})] + \sum_{j=2}^{\infty} \frac{T^j [(a_j^{ns} - a_j^{ws})]}{j-1} \right] \tag{32}$$

Ignoring the higher order terms ( $j > 1$ ) and substituting  $\beta_0 = a_0^{ns} - a_0^{ws}$ ,  $\beta_1 = c^{ns} - c^{ws}$  and  $\beta_2 = a_1^{ns} - a_1^{ws}$  we get,

$$p^c(T) = \frac{2}{r} [\beta_0 + \beta_1 T + \beta_2 T \ln T] \tag{33}$$

Grant [66] discusses the rationale behind ignoring the higher-order terms, and readers are encouraged to refer to their work for finer details of the derivation. The truncated expression relating the capillary pressure at a target temperature ( $T_f$ ) to a reference temperature ( $T_r$ ) is given by,

$$p_{T=T_f}^c = p_{T=T_r}^c \left( \frac{\beta_0 + T_f + \beta_2 T_f \ln T_f}{\beta_0 + T_r + \beta_2 T_r \ln T_r} \right) \tag{34}$$

where  $\beta_1 \approx 1$  [43]. The above two-parameter expression reduces to Grant and Salehzadeh’s [43] one-parameter expression (Eq. (25)) when  $\beta_2 = 0$ . It would be appropriate to make this assumption over a small temperature range since the  $\ln$  term changes slowly. However, over higher temperature ranges, the  $\ln$  term may contribute significantly to the overall capillary pressure change and hence should not be ignored.

The two-parameter model fits the available water–air capillary pressure data slightly better than the one-parameter model [66]. For the drainage data of silica sand reported by She and Sleep [67], Grant [66] estimated the  $\beta_0$  and  $\beta_2$  values to be  $-86.6$  mN/m and  $-0.134$  mN/mK, respectively. The  $\beta$  values are valid between 20 and 80 °C, which is the temperature range for which measurements were made. The models fit well the experimental data for heterogeneous porous media like soils and homogeneous porous media like uniformly composed glass beads. The wide range of applicability of the models is encouraging for using these models for food systems.

The models, however, did not fit the data for water–oil systems as well as they did for the water–air systems. In some cases, the standard errors in estimates were of the order of the estimate. Nevertheless, expressions to estimate the temperature sensitivity of capillary pressure are promising with regard to the ease of their implementation in mathematical models. Capillary pressure data for food systems at different temperatures would be needed to estimate the fit of these proposed models, and experimental work for food systems is encouraged.

The motivation for this section was to discuss some expressions developed for the temperature dependence of capillary pressure based on interfacial thermodynamics. Some other such relationships have been summarized by Kang and Chung [44]. Though not all the available expressions have a theoretical basis in interfacial phenomenon, the ultimate choice is left to the reader. Capillary pressure data for food systems at different temperatures would be needed to estimate the fit of these proposed models.

## Capillary Pressure Measurement in Foods

The commonly used methods for measuring capillary pressure include the high-speed centrifugation technique, porous plate technique, and mercury injection technique. An in-depth description of these techniques, including sample preparation, test equipment, procedure, advantages, and limitations, can be found in McPhee et al. [68]. These techniques were developed for geological and soil sciences applications, which deal with rigid and non-cellular structures [69]. Most solid food materials are essentially soft biopolymeric matrices that would deform under stress. This is especially true for experiments involving the application of a high-pressure or centrifugal force to drive liquid flow from the food. Deformation of food can lead to a structural breakdown, which might affect the results. Additionally, methods that require long contact times with water to attain equilibrium may lead to microbial spoilage and swelling of the food sample [53]. Thus, there are challenges in adopting currently available capillary measurement techniques to foods. As a result, very little capillary pressure data is available in the food literature. Nevertheless, some studies involving capillary pressure estimation in foods have been discussed in this section. The idea is to encourage further development of capillary pressure measurement methods specific to food systems. Broadly, the available methods can be grouped as direct or indirect measurements.

### Direct Measurement

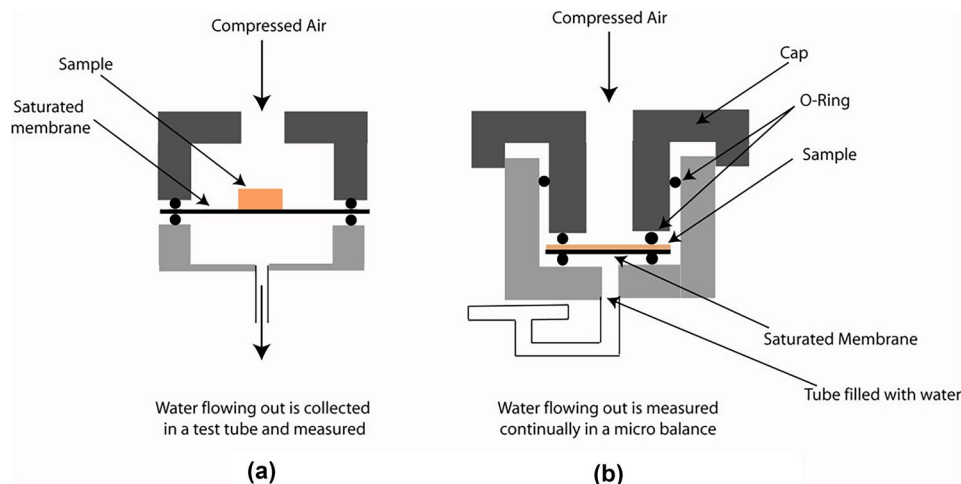
Direct measurement techniques measure the capillary pressure developed in a food matrix directly. One such attempt was made by Halder et al. [69] for potatoes. The capillary pressure measurements were made using pressure plate (porous plate) experiments and liquid extrusion porosimetry. The setup for both methods is shown in Fig. 8. It was

assumed that liquid (water) flow is induced as long as the applied pressure is greater than the capillary pressure. As the food loses moisture, the capillary pressure in the food matrix is expected to increase. When the capillary pressure equals the applied pressure, no water flows from the food. Measurements are made at different applied pressures, and the corresponding moisture contents are noted in order to make a capillary pressure-moisture content curve. For the pressure plate experiments, the samples were allowed to equilibrate in a 100%RH pressure chamber for 5 days at pressures up to 1.5 MPa, which was the maximum possible for the equipment. In the case of the porosimeter, the pressure was raised every hour by 0.025 MPa till the applied pressure reached the maximum possible value of 0.7 MPa. The intermediate moisture contents are estimated by measuring the drained water at fixed intervals. In both experiments, only 2% of the total water flowed out at the maximum possible pressure. Some explanations cited for these observations include the development of high capillary pressures (higher than the maximum applied pressure) and the presence of a larger fraction of water inside cells than in the capillaries. Furthermore, capillary pressure experiments at higher temperatures were restricted by the softness of potatoes at those temperatures. Thus, equipment capable of driving out all the water in the capillaries without causing deformation is needed to measure the capillary pressure.

### Indirect Measurement

Indirect measurement techniques use measured quantities like pore radius, contact angle, surface tension, and water activity to estimate the corresponding capillary pressure. This estimation is done using capillary pressure formulae like the Young–Laplace equation (Eq. (13)) or the Kelvin equation (Eq. (37)). Stevenson et al. [70] estimated the capillary pressure in polyacrylamide gels and minced chicken breast gels

**Fig. 8** Setup for direct capillary pressure measurement using **a** pressure plate, **b** liquid extrusion porosimeter (reprinted from Halder et al. [69] with permission from John Wiley and Sons)



using the Young–Laplace equation. Pore size measurements were made using scanning electron microscopy (SEM) combined with image analysis, and the contact angle was measured using the captive bubble method. The surface tension was assumed to be equal for all samples and equal to the standard surface tension of water at 20 °C, i.e., 72.86 mN/m. The estimated capillary pressure for polyacrylamide gels and chicken meat gels was of the order of 10 MPa, with the highest calculated capillary pressure just above 90 MPa. This approach has some limitations. First, it uses the macroscopic form of the Young–Laplace equation, which itself has some limitations, as described in “[Macroscale Definition](#).” Second, it uses mean values of pore diameter and contact angles for capillary pressure estimation. Solid foods generally have non-homogeneous porous structures with varying pore sizes and non-uniform contact angles. Third, it uses the standard surface tension of water. The authors admit that surface tension can be affected by the presence of solutes like salts, sugars, and preservatives. Thus, a measurement of surface tension for the solution inside the gel must be made for better predictions of the capillary pressure.

Weerts et al. [8] studied the rehydration kinetics of dried green tea at different temperatures. They emphasized that hydration is not a diffusive process but is rather driven by capillary flow. To solve the unsaturated transport equation for water uptake, a water retention curve that expresses the capillary potential as a function of saturation is needed. van Genuchten’s [48] expression (Eq. 15) was selected for this study. In order to find the fitting parameters  $\alpha$  and  $n$ , the Kelvin equation (Eq. (39)), which expresses the capillary head as a function of water activity, is inserted in the van Genuchten expression. The least-square values of  $\alpha$  and  $n$  were determined using the saturation-water activity data adapted from a moisture sorption isotherm available for tea. Good fits were obtained (Fig. 5), and this procedure was performed for four different temperatures. The optimum  $\alpha$  and  $n$  values are summarized in Table 1. The approach used in this study estimated the capillary potential without actually measuring it, hence not facing the same problems as direct measurement techniques. Also, moisture sorption isotherms are widely available for different foods and at various temperatures. However, a word of caution is necessary regarding the use of the Kelvin equation to relate the capillary potential and water activity. The applicability of the Kelvin equation is widely contested. This is discussed further in “[Kelvin Capillary Penetration](#).” As a result, this indirect approach may face the same challenges of applicability.

A similar approach was adopted by Troygot et al. [53] for modeling the rehydration kinetics of a model food system made from microcrystalline cellulose (MCC). The commonly used capillary pressure expressions perform poorly for lower water saturations [53]. It was assumed that the capillary pressure at lower saturations is a linear function of wetting phase

saturation when plotted on a semilog plot. The Brooks–Corey expression Eq. (19) was merged with the exponential estimation of capillary pressure (for lower water saturations) to get the so-called merged moisture characteristic curve. It was further assumed that the merged curve intersects the capillary head axis at  $10^5$  m. The point where the two curves merge is determined by imposing the continuity requirement, i.e., equal slopes. Using available water sorption isotherm data,  $\lambda$  (fitting parameter for Brooks–Corey expression) was estimated. The rehydration kinetics of MCC was predicted well using the merged moisture characteristic curve.

## Mathematical Models for Food Systems

In general, mathematical models for food systems can either be developed based on an in-depth understanding of the physics or alternatively can be conceptualized essentially as functions that produce outputs that agree reasonably well with experimental results when provided a set of input variables corresponding to the experimental conditions. In either case, the objective is to predict the outcomes of a process. The latter type of model, known as empirical models, is, in most situations, much easier to develop and implement. However, these models often need a large amount of experimental data and do not provide insights into the underlying physical mechanisms. As food engineers and scientists, it is interesting to explore the physical phenomenon behind processes, and the fundamental knowledge on mechanisms helps to improve the processes. This is generally not possible employing empirical models. As a result, the discussion about empirical models has been excluded from this paper.

Physics-based modeling starts with accounting for the different phenomena that occur simultaneously in a system. This represents one of the biggest challenges because not all processing techniques have been explored sufficiently to determine all such phenomena, let alone derive governing equations to represent them. Most mechanistic models rely on certain simplifying assumptions by ignoring certain phenomena which may not contribute significantly to the overall process. For example, some models account for capillary flow explicitly, while some models combine it with other flows, thus making it indistinguishable. A range of such mechanistic models has been discussed in this section.

There is no single agreed-upon model that can satisfactorily account for all the fluid flow phenomena and performs accurately without requiring certain assumptions or parameter fitting using available experimental data. Nevertheless, a clear distinction and comparison can be made between different models.

The following are examples of models used for modeling liquid flow in unsaturated porous structures: (i)

Lucas-Washburn capillary penetration, (ii) Kelvin capillary penetration, (iii) combined diffusion, and (iv) capillary diffusion. Though the aim is not to single out any one formulation, the ease of use and drawbacks of each formulation will be discussed briefly.

### Lucas-Washburn Capillary Penetration

The Lucas-Washburn model estimates the capillary penetration for a highly simplified version of porous media transport. A porous medium can be modeled as a bunch of fine cylindrical capillaries with an average or effective capillary radius. The capillary pressure which develops in such a capillary placed in an infinite liquid reservoir is balanced mainly by the viscous and gravity forces [1, 71]. The force balance equation, ignoring the inertial term, is given by [71],

$$\frac{dh}{dt} = \left( \frac{r\gamma \cos \theta}{4\mu h} \right) - \frac{r^2 \rho g \cos \beta}{8\mu} \quad (35)$$

where  $h$  is the capillary pressure head,  $r$  is the capillary radius,  $\gamma$  is the interfacial tension between the wetting and non-wetting phase,  $\rho$  and  $\mu$  are the density and viscosity of the wetting phase,  $g$  is the gravitational acceleration,  $\theta$  is the contact angle, and  $\beta$  is the angle formed by the capillary tube with the vertical direction ( $\beta = 0$  for vertical capillary). Integrating the above equation (Eq. (35)) for a horizontal capillary tube ( $\beta = \pi/2$ ) gives,

$$h = \sqrt{\frac{r\gamma \cos \theta t}{2\mu}} = Gt^{\frac{1}{2}} \quad (36)$$

where  $G = \sqrt{\frac{r\gamma \cos \theta}{2\mu}}$

The same expression is obtained for any angle  $\beta$  when the gravitational forces are not significant contributors.

Aguilera et al. [1] argued that diffusive transport based on Fick's 2nd law has been used extensively but incorrectly to model the fat migration in chocolates. They hypothesized that the particulate nature of chocolate leads to the development of capillary forces, which drive the movement of the liquid fraction of cocoa fat. They proposed using the Lucas-Washburn model to predict the movement of fat in chocolate. They showed that the analytical solution for both Fickian diffusion and the Lucas-Washburn model has a square root of time dependency with respect to mass transfer. However, it must be emphasized that both models are fundamentally different. Fat migration leads to major quality problems like fat blooms and softening of coatings. This necessitates the development of such capillary flow-based predictive models to optimize processing and storage techniques.

Lee et al. [15] studied the rehydration of freeze-dried avocado, kiwi, apple, banana, and potato using the

Lucas-Washburn model. Reasonable agreement was found between the measured and calculated capillary rise in the samples. They also showed that the rehydration rate of freeze-dried avocados was nearly two orders of magnitude greater than that for tray-dried avocados, showcasing the superior reconstitution qualities of freeze-dried foods. However, like most studies that use the Lucas-Washburn model, several simplifying assumptions were made.

A one-dimensional, fully developed Newtonian (laminar) flow in a perfectly cylindrical straight capillary with an effective (representative) radius is assumed. Furthermore, the advancing contact angle is assumed to be constant and equal along all capillaries [72]. Additionally, the model does not account for the swelling of the matrix and its effect on the capillary flow. Each of these assumptions is a probable source of the erroneous nature of the model.

Capillaries in porous media like foods are rarely straight and further develop tortuosity during processing operations like drying or frying. Carbonell et al. [73] studied the movement of sunflower oil through packed beds of chocolate crumbs using a modified version of the Lucas-Washburn model by including a tortuosity factor that accounts for the longer flow path.

Porous structures like foods have a wide range of pore sizes and pore geometries. Using a statistically determined effective radius cannot account for this pore size distribution and its impact on the capillary flow. The pores also undergo changes during processing, as was shown by Alam and Takhar [32] for frying ("Pore Radius"). Also, it is difficult to justify the assumption that contact angles within and across capillaries are constant and equal, respectively [74]. The effect of matrix swelling and its impact on flow through a change in pore radius is challenging to account for but is another source of error. In fact, since the derivation of the model uses the upscaled Young-Laplace equation [75], there are bound to be deviations between predicted and observed behavior (discussed in "Macroscale Definition").

Saguy et al. [76] found non-conforming results (predicted vs. experimental) for the rehydration of freeze-dried carrots studied using the Lucas-Washburn model. They highlighted the simplifying assumptions in the Lucas-Washburn model as the source of discrepancies. Specifically, significant swelling of the carrot matrix was seen in the images taken during the rehydration experiment. This is expected to change the pore radius and subsequently affect the capillary flow behavior. Lastly, good data for contact angle, viscosity, and surface tension in food systems is generally unavailable, further complicating the use of the Lucas-Washburn model.

Since the aim is to develop a realistic mathematical model which does not rely on as many assumptions as made in the Lucas-Washburn model, it is suggested to use some other formulation for capillary-driven flow.



## Kelvin Capillary Penetration

William Thomson (Lord Kelvin) studied the difference in vapor pressure over curved and planar interfaces between a liquid and its vapor. The exponential form of the Kelvin equation derived using a force balance across the interface at equilibrium is given by [77],

$$\frac{P}{P_0} = \exp\left(\frac{M_w}{\rho_l R} \frac{1}{T} \frac{2\gamma}{R_c}\right) \quad (37)$$

The approximate or linear form is given by [77],

$$\frac{P}{P_0} = 1 + \frac{M_w}{\rho_l R} \frac{1}{T} \frac{2\gamma}{R_c} \quad (38)$$

Here,  $P$  is the vapor pressure over the meniscus,  $P_0$  is the vapor pressure over the planar surface,  $T$  is the temperature,  $R_c$  is the radius of curvature of the liquid surface in the tube,  $M_w$  is the molecular weight,  $\rho_l$  is the liquid density, and  $R$  is the universal gas constant.

An alternative form that expresses the capillary pressure in terms of the water activity is given by [78],

$$P^c = -\frac{RT}{v_w} \ln(a_w) \quad (39)$$

where  $a_w$  is the water activity and  $v_w$  is the molar volume of water ( $\text{m}^3 \text{mol}^{-1}$ ). Water activity is easy to measure, and extensive work relating the water activity to moisture content (sorption isotherms) has been done. The rehydration kinetics study of dried green tea carried out by Weerts et al. [8] using the Kelvin equation (Eq. (39)) has been discussed in “[Indirect Measurement](#).”

Liquid bridging followed by caking represents a major quality problem during the storage and transport of sucrose. Liquid bridging is initiated by capillary condensation in pores or capillaries formed between adjacent sucrose crystals in a packed bed [79]. The Kelvin equation can predict the critical capillary radius below which capillary condensation will take place readily. Billings et al. [79] showed that the critical capillary radius increased exponentially beyond a water activity of 0.8. Thus, the increased tendency to form liquid bridges beyond this water activity also increases the chances of caking. Storage and transport conditions that maintain water activity below 0.8 are recommended to prevent sucrose caking.

Rosa et al. [80] estimated the pore size distribution for chitosan using the Kelvin equation. The Kelvin equation does not account for the thickness of the precondensation film on the pore walls and needs to be combined with the Halsey equation (not discussed here) for the correct prediction of pore sizes [80]. The calculations were done at 60°C, the industrial drying temperature for chitosan. The average pore size for chitosan was found to vary from 0.5 to 30 nm at different moisture contents.

Labuza and Rutman [81] investigated the effect of surface-active agents on the sorption behavior of a model food system (made from microcrystalline cellulose, a high molecular weight hydrocarbon oil, water, and surfactant). By employing the Kelvin equation, it was shown that a lowering in the air–liquid surface tension due to surfactants increased the water activity of the system at the same moisture content and diminished the magnitude of hysteresis in the sorption curve.

However, a great deal of work has gone into proving the applicability of the equation and, conversely, the reasons for observed inaccuracies of the equation [82–86]. More specifically, predicted and observed data agree well for droplets, but there seem to be discrepancies in the predictions for capillaries, which is of more interest to us [82].

As cited by Al-Rub and Datta [82], earlier studies of Shereshefsky [87], Shereshefsky and Carter [88], Folman and Shereshefsky [89], Coleburn and Shereshefsky [90], McGavack and Patrick [91], Everett and Whitton [92], and Pierce et al. [93] also found non-agreeing results. The reason for such differences has been hypothesized to be due to the interaction between the solid capillary and the liquid. These surface forces have not been accounted for in the Kelvin equation, leading to inaccuracies. Since such forces would be absent or negligible for droplets, the Kelvin equation works reasonably well for such cases. However, the assumption of an inert porous matrix may be erroneous, especially for biopolymeric matrices like food. Al-Rub and Datta [82] modified the Kelvin equation based on thermodynamics to account for the long-range surface forces.

However, given the wide body of evidence collected through studies that have found problems in the applicability of the Kelvin equation, it may be better to avoid using the Kelvin equation for accounting for the capillary-driven transport in a mathematical model. Although derived based on the physics at the interface, unless the surface forces are accounted for satisfactorily, using the Kelvin equation may reduce the overall predictive power of the model.

## Combined Diffusion

Ficks’s law–based modeling of diffusive transport of fluids (Eq. (40)) has been used extensively in the literature, especially when a deeper understanding of capillary flow was missing. Fick’s law can be written as:

$$\frac{\partial C}{\partial t} = \nabla \cdot (D_{eff} \nabla C) \quad (40)$$

Here,  $C$  is the liquid concentration and  $D_{eff}$  is the effective diffusivity. It is a simplistic and convenient way to model many common food processing operations like hot air drying, microwave drying, hydration/rehydration, frying, and baking [94, 95, 76, 96, 97].

Equation (40) is commonly simplified by making certain assumptions like concentration-independent diffusivity, isothermal conditions, isotropy of material, and negligible volume changes [95]. Furthermore, regular geometries like spheres, cylinders, or slabs are considered. Equation (40) simplified for a sphere with radial diffusion is given by,

$$\frac{\partial C}{\partial t} = D_{eff} \left( \frac{\partial^2 C}{\partial r^2} + \frac{2}{r} \frac{\partial C}{\partial r} \right) \quad (41)$$

The analytical solution to Eq. (41), as derived by Crank [98], is given by,

$$\frac{C - C_1}{C_0 - C_1} = 1 + \frac{2a_s}{\pi r} \sum_{n=1}^{\infty} \frac{(-1)^n}{n} \sin \frac{n\pi r}{a_s} \exp \left( \frac{-D_{eff} n^2 \pi^2 t}{a_s^2} \right) \quad (42)$$

where  $C_0$  is the constant surface concentration,  $C_1$  is the initial uniform concentration, and  $a_s$  is the radius of the sphere. Here, additional assumptions have been made, which include uniform initial moisture content, instantaneous equilibrium moisture content at the surface, and symmetric mass transfer with respect to the center [96].

An analytical solution to the problem was found by making many assumptions. Making such assumptions weakens the model, and it is recommended to avoid as many assumptions as possible. With the increased availability of sophisticated numerical packages, it has become much simpler to account for most complexities.

Experimental data is needed to estimate the effective diffusivity. The effective diffusivity can be determined using optimization algorithms that minimize the sum of squared errors between the experimental and model-predicted moisture contents [95].

Zhang et al. [14] studied the moisture loss kinetics during deep frying of battered and breaded fish nuggets at three temperatures (160, 170, and 180 °C). The moisture loss from the crust was modeled by fitting the experimental data of the crust to Fick's second law of diffusion, and the effective moisture diffusivity was estimated. The nugget could not be modeled as an individual entity since it was battered and breaded. The crust was modeled as an infinite slab, and it was assumed that the external resistance to mass transfer was negligible. The effective moisture diffusivity was found to increase with temperature (160 to 180 °C) from  $5.05 \times 10^{-9}$  to  $5.81 \times 10^{-9}$  m<sup>2</sup>/s.

Cazzaniga et al. [12] estimated the effective moisture diffusivity for baking cassava snacks at four temperature–time combinations (190|14, 205|9, 220|9, and 235|6 °C|min). Samples were prepared by substituting wheat flour for different dehydrated cassava puree proportions. The effective diffusivity ranged from  $5.22 \times 10^{-6}$  m<sup>2</sup>/s to  $2.93 \times 10^{-5}$  m<sup>2</sup>/s. Formulations with dehydrated cassava puree had higher effective diffusivities, though no clear trend was observed

with respect to the proportion of wheat flour replaced. The high magnitudes of effective diffusivity were hypothesized to be due to the high initial moisture content of the doughs, the small volume of the samples, and high baking temperatures, which may lead to the faster formation of a porous structure.

$$D_{eff} = A \exp \left( -\frac{E_a}{RT} \right) \quad (43)$$

Several different expressions are available in the literature to express the temperature dependence of effective diffusivity. Suarez et al. [97] studied the drying of sorghum and determined the effective moisture diffusivity at different drying temperatures. Using an Arrhenius-type equation (Eq. (43)), the activation energy ( $E_a$ ) for diffusion in Sorghum was estimated to be  $31.38 \frac{\text{kJ}}{\text{gmol}}$ . Here,  $A$  is the pre-exponential factor. Demiray and Tulek [13] used a similar approach to analyze the effect of temperature on the rehydration kinetics of sun-dried red pepper. The activation energy was estimated to be  $3.17 \frac{\text{kJ}}{\text{gmol}}$ .

The effective diffusion model accounts for all different flows by lumping them into an effective diffusivity, which is inversely determined. Additionally, no distinction is made between the flow of water and water vapor. Rather, the collective “moisture” flow is modeled. It is now clear that vapor flow is driven by gas pressure and molecular diffusion, and liquid flow is majorly driven by gas and capillary pressure. It is thus erroneous to consider a combined flow of both phases.

The unavailability of rigorous constitutive relationships to account for matrix interactions, especially in the food literature, forces the use of an effective diffusion model [8]. However, an improved understanding of fluid flow in porous food structures has made it possible to model physics more accurately.

## Capillary Diffusion

Unlike the effective or combined diffusion formulation, where the water and vapor transport are clubbed into a diffusion term, the capillary diffusion formulation uses a capillary diffusivity term to account for the capillary-driven flow of liquid. Therefore, both gas pressure and capillary-driven liquid flow are accounted for in the model. More details about this type of formulation can be found in the work of Datta [5, 99], Halder et al. [100], Ni and Datta [101], and Ni et al. [102]. The mass flux of the liquid is written using Darcy's law as [5],

$$j_m = -\rho^l \left( \frac{K^l}{\mu^l} \right) \frac{\partial(p^g - p^c)}{\partial s} = -\rho^l \left( \frac{K^l}{\mu^l} \right) \frac{\partial p^g}{\partial s} + \rho^l \left( \frac{K^l}{\mu^l} \right) \frac{\partial p^c}{\partial s} \quad (44)$$

Here, the gas pressure ( $p^g$ ) can be seen as the “pushing” force and the capillary pressure ( $p^c$ ) as the “impeding”

force. Thus, the difference in these forces drives the liquid flow. The gas pressure increases to large magnitudes during processes like frying and microwave drying due to strong internal evaporation. The gas pressure dominates the liquid flow in such cases. However, in applications involving significant water removal (e.g., drying) or the use of very dry porous material (powder rehydration), the capillary pressures can rise to very high magnitudes. This can be seen by the behavior of  $hvsS_e$  curve at low saturation values (Fig. 6).

Capillary pressure is dependent on a wide range of factors, but concentration (saturation) and temperature represent two of the most significant factors. Equation (44) can further be written as [5],

$$j_m = -\rho^l \left( \frac{K^l}{\mu^l} \right) \frac{\partial p^g}{\partial s} + \rho^l \left( \frac{K^l}{\mu^l} \right) \frac{\partial p^c}{\partial c^l} \frac{\partial c^l}{\partial s} + \rho^l \left( \frac{K^l}{\mu^l} \right) \frac{\partial p^c}{\partial T} \frac{\partial T}{\partial s} \quad (45)$$

Or rewritten as,

$$j_m = -\rho^l \left( \frac{K^l}{\mu^l} \right) \frac{\partial p^g}{\partial s} - D_c \frac{\partial c^l}{\partial s} - D_T \frac{\partial T}{\partial s} \quad (46)$$

where

$$D_c = -\rho^l \left( \frac{K^l}{\mu^l} \right) \frac{\partial p^c}{\partial c^l}$$

$$D_T = -\rho^l \left( \frac{K^l}{\mu^l} \right) \frac{\partial p^c}{\partial T}$$

Here,  $D_c$  and  $D_T$  are the capillary diffusivities. The concentration and temperature effect on capillary pressure-driven flow have been separated in Eqs. (45) and (46). It is, however, important to mention that though the term diffusivity is being used, the flow is capillary-driven and is only analogous to the diffusivity in Fick's law of diffusion.

The capillary diffusivity formulation has been applied to model a wide range of processes. Using the capillary diffusivity approach, Halder et al. [100, 103] modeled the deep-fat frying of restructured potato slices, Gulati et al. [104] studied the microwave drying of potato cubes, Warning et al. [105] developed a model for deep-fat vacuum frying of potato chips, and Rakesh et al. [106] studied microwave combination heating of cylindrical samples made from rehydrated instant mashed potatoes. As can be seen from the above examples, the capillary diffusivity-based formulations allow the coupling of multiple physics like fluid transport, energy transfer, microwaves, and even poromechanics (predicting food deformation). This represents a significant advantage of this method over other mathematical models for food systems.

The capillary diffusivities depend not just on the change in capillary pressure with temperature and concentration but

also on the density, viscosity, and permeability (Eq. (46)). All of these properties themselves have variable magnitudes. It is thus difficult to find an appropriate expression for the capillary diffusivity in the literature that accounts for all variabilities accurately.

Inverse estimation of capillary diffusivity adds an empirical nature to the model and makes the model specific for a given system and operating conditions. Furthermore, the temperature gradient-driven flow is considered less important as compared to the concentration-driven flow. Thus, the temperature-dependent term is ignored. In sum, only saturation-driven capillary flow is accounted for in the model. Consequently, only concentration-dependent capillary diffusivity values are determined. Even so, there is a dearth of such data in the food literature. Additionally, a single expression that is valid from low to high moisture contents is hard to determine. One such expression developed by Ni [107] for potatoes is given by,

$$D_w = 10^{-8} \exp(-2.8 + 2M) \quad (47)$$

where  $M$  is the moisture content on a dry basis and the unit of  $D_w$  is  $\text{m}^2/\text{s}$ . Once such expressions are determined, their use in mathematical models is fairly straightforward. However, the clubbing of temperature-dependent terms in the diffusivity term, separation of concentration and temperature effects, and the current lack of available capillary diffusivity data make this formulation hard to use for all cases.

## Hybrid Mixture Theory (HMT)

HMT-based models have a strong basis in porous media physics. It is a highly generalized fundamental approach that can be adopted for modeling a wide range of processes. Its application is not just limited to soil and food systems but can be applied to other porous structures as well. Furthermore, it can be adapted to model both saturated and unsaturated porous systems, summarized in Table 2. The work on saturated systems where the pores are completely filled with the liquid phase has progressed much faster than unsaturated systems. The ease of modeling the former is one of the primary reasons for this.

Unsaturated systems have liquid and gas phases occupying the void space. This coexistence of a wetting and non-wetting phase leads to capillary pressure-driven transport in unsaturated systems and makes the study of such systems more complicated. Takhar's [110] work on unsaturated fluid transport in swelling biopolymers allows developing a mechanistic understanding of several food processes.

The HMT approach upscales the microscale conservation laws for mass, momentum, and energy to mesoscale or macroscale. There are two major reasons for deriving equations

**Table 2** HMT-based models developed for studying food processes

Unit operation	Food	Geometry	Saturated/ unsaturated	Capillary pressure expression (air–water)	Deformation	Reference
Drying	Corn kernels	3D kernel geometry using X-ray CT	Saturated	-	Yes	Takhar [108], Takhar et al. [109]
Frying	Rice crackers	2D symmetric rectangle	Unsaturated	$P^c(S^w, T) = (77.5 - 0.185 \times 10^{-3} (T - 273.15)) \left( \frac{3105}{S^w + 10^{-4}} - \frac{1047 - 3.368\rho^s}{1.02 - S^w} + 149.8\rho^s(1 - S^w) + 52.35 + 168.4\rho^s - \frac{3150}{1 + 10^{-4}} \right) \text{Pa}$	No	Bansal et al. [9]
Frying	Potatoes	2D axisymmetric cylinder	Unsaturated	$P^c(S^w) = 0.84 \times 10^5 S^w - 0.63 \text{Pa}$	No	Takhar [110]
Extrusion	Corn starch	2D axisymmetric cylinder	Unsaturated	$P^c(S^w, T) = 101325 [12.12 S^w \exp(-5.939 S^w + 0.046(1 - S^w) S^w - 3.7) \times [1 - 2.79 \times 10^{-3} (T - 273)] \text{Pa}$	Yes	Ditudompo and Takhar [10]
Frying	Chicken nuggets	2D axisymmetric disc	Unsaturated	$P^c(S^w) = 0.84 \times 10^5 S^w - 0.63 \text{Pa}$	No	Bansal et al. [111]
Frying	Potatoes	2D axisymmetric disc	Unsaturated	$P^c(S^w) = (0.128005 - 0.185 \times 10^{-3} (T - 273.15)) \times \left( \frac{3150}{S^w + 0.1e^{-3}} - \frac{5627.48}{1.02 - S^w} + 481.952.315 - 203.728 S^w \right) \text{Pa}$	No	Sandhu and Takhar [112]
Drying	Strawberries	2D axisymmetric disc	Saturated	-	Yes	Ozturk and Takhar [113]
Drying	Carrots	2D axisymmetric disc	Saturated	-	Yes	Ozturk and Takhar [113]
Freezing and freeze–thaw cycles	Potatoes	2D symmetric rectangle	Unsaturated	$P^c(S^w) = 0.84 \times 10^5 S^w - 0.63 \text{Pa}$	Yes	Zhao et al. [11]

at higher scales. Firstly, the material properties, like density, conductivity, and specific heat, are not feasible to measure at the microscale but can be measured experimentally at the macroscale. Secondly, enormous computational resources are saved when the equations are solved for macroscopic representative elementary volumes (REV) instead of working at microscale dimensions. Takhar [110] discusses the loss of some microscale information during the averaging procedure, but the advantages outweigh this.

A significant advantage of the HMT approach developed by Takhar [110] over other models present in the literature is that it accounts for the interaction between the fluid phases and the viscoelastic biopolymeric matrix. Additionally, the cross-effect terms, i.e., the terms which account for the effect on the transport of one phase by the presence of other phases, further make HMT-based mathematical models more robust and accurate.

Some simplifying assumptions are made. A local thermal equilibrium is assumed between the various phases present in a macroscale REV. As a result, a single energy balance equation with volume-averaged material properties is needed. Large spatial variations in temperature are still permitted. The effect of gravity on fluid flow is considered negligible compared to the other driving forces. The gas phase is assumed to be an ideal mixture of vapor and air. The solid and liquid phases are assumed incompressible at the microscale, whereas the gas phase is assumed to be compressible. Macroscale matrix expansion or shrinkage is still permitted [111, 10].

$$v^{\alpha s} = -\epsilon^\alpha \left( \frac{K^\alpha}{\mu^\alpha} \right) \nabla p^\alpha - \epsilon^\alpha D^\alpha \nabla \epsilon^\alpha - \frac{\epsilon^\alpha D^\alpha}{E} B \nabla \epsilon^\alpha, \text{ where } \alpha = w, o, g \tag{48}$$

$$\frac{D^s(\epsilon^\alpha \rho^\alpha)}{Dt} + \nabla \cdot (\epsilon^\alpha v^{\alpha s} \rho^\alpha) - \frac{\epsilon^\alpha}{\epsilon^s} \dot{\epsilon}^s \rho^\alpha = \sum_{\beta \neq \alpha} \beta \hat{c}^\alpha \tag{49}$$

Once the generalized upscaled equations are derived, using entropy inequality [114], the equilibrium, near-equilibrium, and non-equilibrium relations are presented. The resulting generalized Darcy’s law (Eq. (48)) and mass balance equation (Eq. (49)) form the base of the mathematical model [110]. The dot over a variable represents the material time derivative with respect to the solid phase. According to the generalized Darcy’s law (Eq. (48)), the liquid flow relative to the solid matrix is driven by a pressure gradient, concentration gradient, and a time-dependent resistance of polymers to flow. The gas phase flow is driven only by the gas pressure gradient, whereas vapor and air flow are driven by both pressure gradient and binary diffusion. The generalized Darcy’s law provides the expression for velocity that appears in the divergence term of the mass balance equation (Eq. (49)).

$$p^g = p^v + p^a \tag{50}$$

$$\epsilon^s = 1 - \phi \tag{51}$$

The source/sink term on the right-hand side of the mass balance equation accounts for phase changes, for example, between water and vapor, thus coupling their mass balance equations. The source/sink term is a key characteristic of the multiscale model, as this term is generally absent in single-scale models. The liquid phase mass balance equations are solved for the respective volume fractions ( $\epsilon^\alpha$ ), whereas the gas phase mass balance equation is solved for the gas pressure ( $p^g$ ). The vapor mass balance equation is solved for the vapor density ( $\rho^v$ ), and Dalton’s law of partial pressure (Eq. (50)) links the gas ( $p^g$ ), vapor ( $p^v$ ), and air ( $p^a$ ) pressures. The sum of the volume fractions of the fluid phases equals the porosity ( $\phi$ ) of the matrix and the volume fraction of the solid phase ( $\epsilon^s$ ) is given by Eq. (51).

$$\left( \sum_{\alpha=w,o,g} \epsilon^\alpha \rho^\alpha C_p^\alpha \right) \frac{\partial T}{\partial t} + \left( \sum_{\alpha=w,o,g} \epsilon^\alpha \rho^\alpha C_p^\alpha \right) \left( \sum_{\alpha=w,o,g} \epsilon^\alpha v^{\alpha s} \right) \cdot \nabla T = \nabla \cdot \left( \left( \sum_{\alpha=w,o,g} \epsilon^\alpha k^\alpha \right) \nabla T \right) - \lambda_v^w \hat{c}^g \tag{52}$$

Unlike soil and wood, where isothermal conditions can be assumed for many problems, food systems routinely undergo significant temperature changes during processing, which necessitates the coupling of the energy balance equation (Eq. (52)) [25] with the other transport equations. HMT-based models enable such couplings in a simple manner. Energy transfer within the food matrix is driven by convection due to the movement of fluids, conduction, and phase changes.

A wide range of input parameters and material properties, including physical (density, viscosity, diffusivity, permeability), thermal (specific heat, thermal conductivity, latent heat of vaporization), and mechanical properties (elasticity modulus, Poisson’s ratio), are needed. Most of these properties are temperature and concentration-dependent either directly or indirectly. Some of these have been studied more than others. Consequently, appropriate temperature or concentration-dependent expressions may or may not be available in the literature. Accordingly, expressions developed for similar materials may be adopted, or constant values of material properties may be used until further experimental work is available in the literature.

The constitutive relationship of interest, keeping in mind the theme of this paper, is the capillary pressure expression. The capillary pressure is used to calculate the liquid pressure, which appears in the generalized Darcy’s law (Eq. (48)). For example, for the liquid water phase, we have

$$p^w = p^g - P^c(S^w) \tag{53}$$

A  $P^c$  vs  $S^w$  curve is used to estimate the capillary pressure ( $P^c$ ) as the water phase saturation ( $S^w$ ) undergoes spatial and temporal changes during processing. The liquid water phase pressure ( $p^w$ ) is then calculated using Eq. (53).

The complete set of governing equations, including other constitutive relationships required for closure, are then solved using numerical methods such as the finite element method to predict the spatial and temporal variation of moisture, oil uptake, temperature, and pressure, amongst other variables. Examples where the HMT-based model was applied to study frying are discussed in the next section.

## Frying

Historically a lot of work has gone into understanding frying and developing predictive models. Frying represents an unsaturated transport problem with three phases: liquid water, oil, and gas (air + water vapor). The presence of wetting and non-wetting phases leads to the development of capillary pressure in the food matrix. Frying involves evaporation and gas expansion brought about by the heat transfer from the hot oil, typically at 175 – 200°C. Water is lost from the food matrix as vapor, while the oil seeps into the spaces vacated by the water or created by the expanding gas phase. As a result, the saturation of the water phase ( $S^w$ ) decreases while the saturation of the gas ( $S^g$ ) and oil ( $S^o$ ) phase are expected to increase. Consequently, even greater capillary pressure develops in the food matrix, especially in the surface layers, which rapidly lose water to the hot oil. Therefore, capillary pressure-driven transport needs careful consideration when developing mechanistic models to

study frying. Some examples of such models in the frying literature are discussed below.

Halder et al. [100, 103] conducted an extensive modeling study of deep frying. A mechanistic multiphase model based on the capillary diffusivity formulation discussed in “Capillary Diffusion” was developed and applied to predict changes during frying and post-frying for restructured potato samples. A salient feature of the model was the use of a non-equilibrium and distributed formulation of evaporation. The heat and mass transport in the potato slab was solved as an effective 1D problem. The mechanistic model could predict a wide range of variables (phase saturations, temperature, pressure, evaporation rate) and use them to predict important quality parameters like moisture content, oil uptake, crust formation, and acrylamide development during the entire frying process. Model predictions and available experimental data showed good agreement for moisture content, temperature, and crust thickness. It was found that most of the oil uptake occurs during the post-frying phase, and only 24% of the total oil uptake is during frying. Rapid acrylamide generation during high-temperature processing (for example, baking or frying) of potato products is a significant cause of concern, given the carcinogenic potential of this compound [115, 116]. A logistic kinetic model was used for modeling the acrylamide accumulation (generation and degradation) kinetics. Acrylamide degradation was ignored since the temperature inside the sample stays below 180°C; consequently, the degradation is negligible compared to the generation. The predicted total acrylamide content agreed well with the data available in the literature. The predicted spatial distribution of acrylamide showed that the crust region had the

**Fig. 9** Experimental and model predicted moisture content (dry basis) at different frying temperatures (reprinted from Sandhu and Takhar [112] with permission from Elsevier)

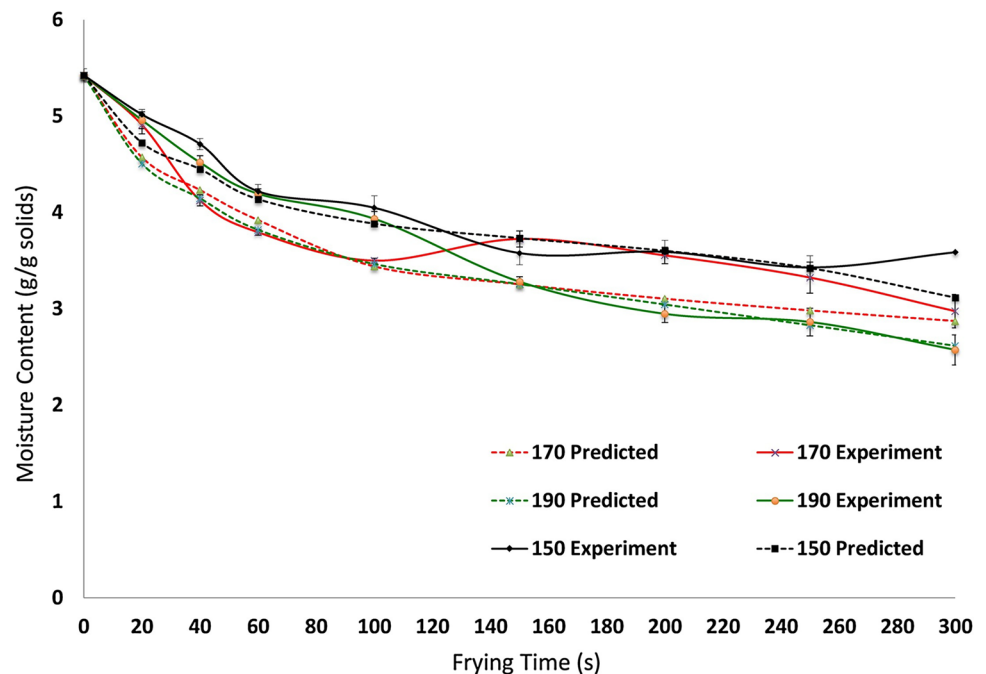
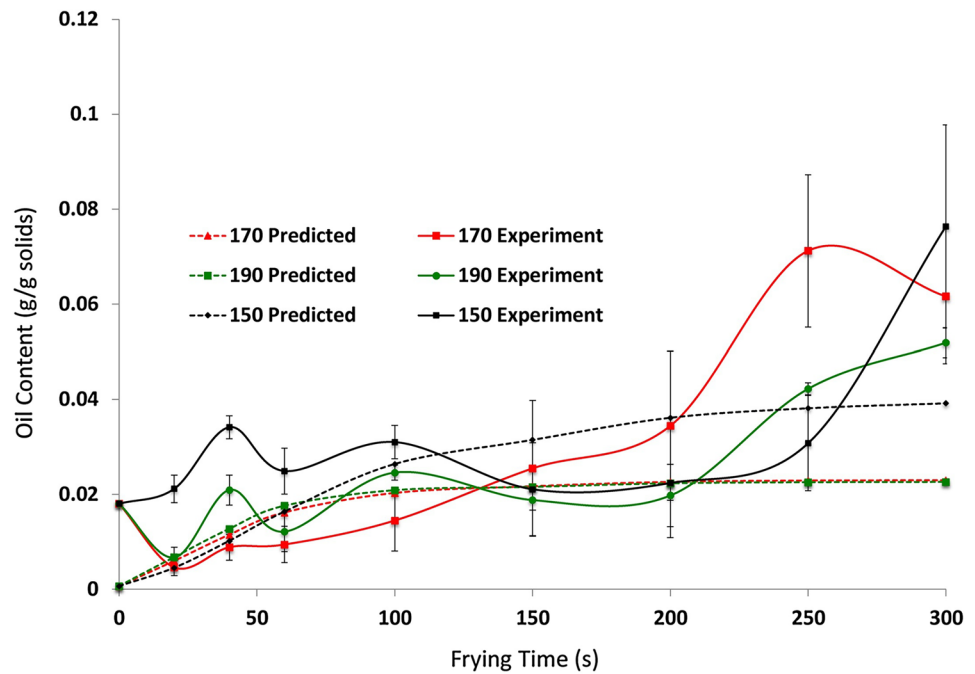


**Fig. 10** Experimental and model predicted oil content (dry basis) at different frying temperatures (reprinted from Sandhu and Takhar [112] with permission from Elsevier)



majority of the acrylamide formation. Experimental pressure measurement data for frying was unavailable; hence, the model predictions were not validated for pressure. The peak gauge pressure predicted by the model was about 800 Pa. According to the pressure measurements made during the frying of potatoes by Sandhu et al. [117] and Parikh and Takhar [118], the peak gauge pressure was much higher (greater than 5000 Pa), as opposed to the lower peak pressure predicted by Halder's [100, 103] model. A sensitivity study performed for the surface mass transfer coefficient and oil capillary diffusivity showed that capillary action is the main driving force for oil uptake.

Sandhu and Takhar [112] verified the two-scale HMT-based model of Takhar [110] by carrying out controlled frying experiments for potato discs. The study is unique in two aspects. First, it uses an insulating Teflon disc to hold the potato disc, which only allows fluid movement through the top and bottom surfaces, thereby making the problem one-dimensional. Second is the accounting for surface oil on the food, which penetrates into the food when the food is taken out of the frying oil. The model predicts only the oil uptake during frying. Thus, by removing the surface oil, a better agreement between the predicted and experimental data was achieved. The validation results for moisture, oil uptake, and temperature for three frying temperatures (150, 170, and 190°C) are shown in Figs. 9, 10, and 11. The model predictions agree well with the experimental data. Plots for predicted spatial variation of moisture, oil uptake, evaporation rate, and gas pressure, which otherwise would be hard to measure experimentally, can also be found in Sandhu and Takhar's [112] work.

Bansal et al. [111] developed an HMT-based model to study the frying of breaded chicken nuggets. Unlike potato discs which are homogeneous and can be modeled as a single domain, breaded chicken nuggets represent a multidomain heterogeneous product. The two domains (coating and meat core) have different material properties. The form of the governing equations remains the same, but there is added complexity in solving the model for the two domains simultaneously while maintaining a continuity of dependent variables like volume fractions, temperature, etc., across the domains. Despite the complexities, a reasonable agreement between predicted and experimental data was found.

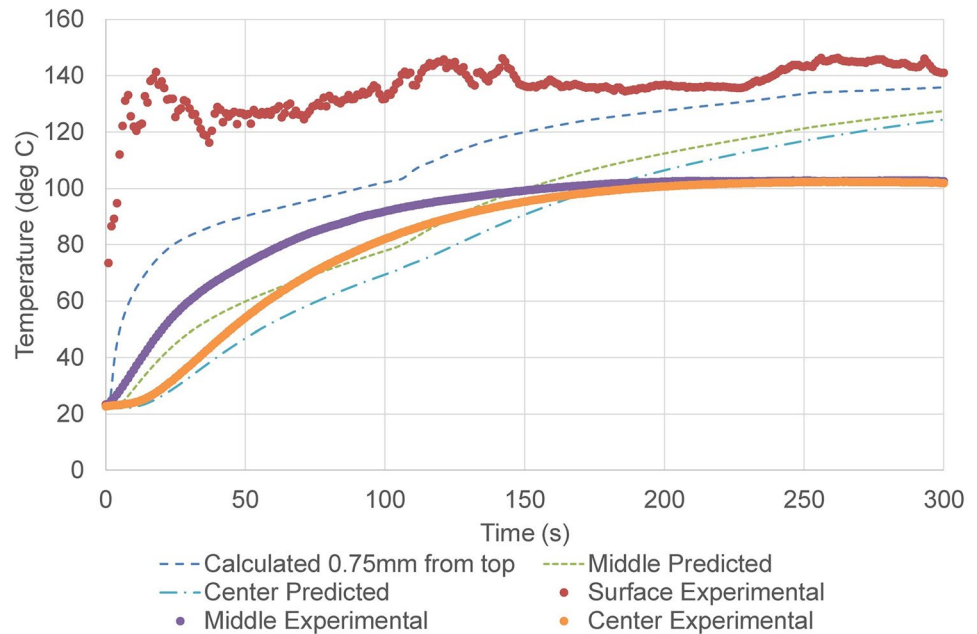
Sandhu and Takhar [112] used the capillary pressure expression determined by Kang and Chung [44] for Softwood, whereas Bansal et al. [111] used the capillary pressure expression determined by Spolek and Plumb [45] for Softwood (Table 2). As has been stressed at multiple points in this paper, there is a dearth of available capillary pressure data for food systems which encourages the adaption of expressions from soil and wood sciences.

The readers are referred to the respective publications for further details about the models like boundary conditions, initial conditions, material properties, solver settings, and the experimental procedures used.

## Limitations

The limitations associated with HMT are not due to any fundamental flaw in the theory or improper mathematical treatments. The requirement of a wide range of material properties and constitutive relationships poses the biggest

**Fig. 11** Experimental and predicted temperature profiles near surface, 2.5 mm from surface and center of potato disc during frying at  $T = 170\text{ }^{\circ}\text{C}$  (reprinted from Sandhu and Takhar [112] with permission from Elsevier)



challenge to HMT-based models, or for that matter, any model developed on fundamental principles.

There is a lack of experimental work done to find appropriate temperature/moisture-dependent expressions for diffusivity, permeability, thermal conductivity, specific heat, density, etc., for food systems. Diffusivity and permeability magnitudes affect the transport equations directly and significantly. A sensitivity test can be done to prove their importance.

The capillary pressure–saturation–temperature relation is another important expression for which insufficient data is available in the food literature. Additionally, even if such expressions are available, their range of validity may not be sufficient to use them directly. For food processes like frying and baking, which involve large temperature changes, material property data may need to be extrapolated to higher temperatures which further adds uncertainty to the results. The model's overall accuracy is an indirect consequence of the accuracy of such expressions. Given the current lack of data, expressions developed for other systems (or other foods) are inversely fitted for the models under consideration. Though this is not an ideal approach, it is a viable option until more experimental work is done.

## Conclusions

This paper reviewed the importance of capillary pressure in unsaturated food systems and the different approaches used to account for capillary pressure–driven flow in mathematical models. The assumptions involved in upscaling the microscale

definition of capillary pressure were discussed. Many studies in the literature use the upscaled definition of capillary pressure, which may be one of the reasons for the deviation between observed and predicted results. The factors affecting capillary pressure, like interfacial tension, contact angle, and pore radius, were reviewed. Most porous solid foods have a non-uniform structure, and as a result, pore radius and contact angle are expected to vary within the food. Similarly, interfacial tension may vary depending on the food formulation. The various available parametric expressions in the literature for capillary pressure as a function of saturation and temperature were listed. These expressions can be implemented in mathematical models in a simple manner. Some studies conducted to estimate the capillary pressure in food systems were presented. Foods may undergo deformation at high pressures, which impedes further experimental work on capillary pressure measurement in foods. As a result, new techniques specifically developed for foods are needed. A wide range of mathematical models for food systems were discussed. Each model has certain limitations, which are mostly related to the simplifying assumptions made while developing the model. At the same time, the ease of use and availability of appropriate material property data may vary across models. Hybrid mixture theory–based models are able to include unsaturated transport mechanisms in foods while accounting for capillary pressure–driven flow and matrix–fluid interactions. Such models based on a rigorously developed theory will allow food engineers to predict the physicochemical changes in foods and consequently optimize existing or develop novel processing techniques. Further work on estimating material properties like diffusivity and permeability will aid the development of such mechanistic models.



**Author Contribution** Y. S. wrote most of the manuscript text, reviewed the literature, gathered the figures, organized the contents, and acquired figure permissions. P. S. T. provided overall guidance, perceived the main idea, provided examples of applications to be incorporated, edited the text, and wrote parts of the manuscript.

**Funding** The USDA-NIFA provided financial support under award numbers 20–67017-31194, ILLU-698–308, and ILLU-698–926.

## Declarations

**Competing Interests** The authors declare no competing interests.

## References

- Aguilera JM, Michel M, Mayor G (2004) Fat migration in chocolate: diffusion or capillary flow in a particulate solid?—a hypothesis paper. *J Food Sci* 69(7):167–174
- Lumen Learning and OpenStax (2021) Fundamentals of Heat, Light & Sound. <https://pressbooks.nsc.ca/heatlightsound/>
- Rahman MM, Gu Y, Karim MA (2018) Development of realistic food microstructure considering the structural heterogeneity of cells and intercellular space. *Food Struct* 15:9–16
- Dadmohammadi Y, Datta AK (2020) Food as porous media: a review of the dynamics of porous properties during processing. *Food Rev Int* 1–33.
- Datta AK (2007a) Porous media approaches to studying simultaneous heat and mass transfer in food processes. I: problem formulations. *J Food Eng* 80(1):80–95
- Shah Y, Takhar PS (2022) Pressure development and volume changes during frying and post-frying of potatoes. *LWT* 172:114243
- Vitrac O, Trystram G, Raoult-Wack AL (2000) Deep-fat frying of food: heat and mass transfer, transformations and reactions inside the frying material. *Eur J Lipid Sci Technol* 102(8–9):529–538
- Weerts AH, Lian G, Martin DR (2003) Modeling the hydration of foodstuffs: temperature effects. *AIChE J* 49(5):1334–1339
- Bansal HS, Takhar PS, Maneerote J (2014) Modeling multiscale transport mechanisms, phase changes and thermomechanics during frying. *Food Res Int* 62:709–717
- Ditadompo S, Takhar PS (2015) Hybrid mixture theory based modeling of transport mechanisms and expansion-thermomechanics of starch during extrusion. *AIChE J* 61(12):4517–4532
- Zhao Y, Kumar PK, Sablani SS, Takhar PS (2022) Hybrid mixture theory-based modeling of transport of fluids, species, and heat in food biopolymers subjected to freeze–thaw cycles. *J Food Sci* 87(9):4082–4106
- Cazzaniga A, Brousse MM, Linares AR (2022) Kinetics of moisture loss applied to the baking of snacks with pregelatinized cassava starch. *J Food Sci*
- Demiray E, Tulek Y (2017) Effect of temperature on water diffusion during rehydration of sun-dried red pepper (*Capsicum annum* L.). *Heat Mass Transf* 53(5):1829–1834
- Zhang W, Chen J, Yue Y, Zhu Z, Liao E, Xia W (2020) Modelling the mass transfer kinetics of battered and breaded fish nuggets during deep-fat frying at different frying temperatures. *J Food Qual* 2020
- Lee KT, Farid M, Nguang SK (2006) The mathematical modelling of the rehydration characteristics of fruits. *J Food Eng* 72(1):16–23
- Vavra CL, Kaldi JG, Sneider RM (1992) Geological applications of capillary pressure: a review. *AAPG Bull* 76(6):840–850
- Shi S, Belhaj H, Bera A (2018) Capillary pressure and relative permeability correlations for transition zones of carbonate reservoirs. *J Pet Explor Prod Technol* 8(3):767–784
- Kaliakin VN (2017) Example problems involving in situ stresses under hydrostatic conditions. In *Soil Mech* (pp. 205–242). Elsevier. <https://doi.org/10.1016/b978-0-12-804491-9.00005-7>
- Pinder GF, Gray WG (2008) Essentials of multiphase flow and transport in porous media. John Wiley & Sons
- Gu Z, Qi Z, Burghate R, Yuan S, Jiao X, Xu J (2020) Irrigation scheduling approaches and applications: a review. *J Irrig Drain Eng* 146(6):04020007
- Yadvinder-Singh Kukal SS, Jat ML, Sidhu HS (2014) Improving water productivity of wheat-based cropping systems in South Asia for sustained productivity. In *Advances in Agronomy* (pp. 157–258). Elsevier. <https://doi.org/10.1016/b978-0-12-800131-8.00004-2>
- Venturas MD, Sperry JS, Hacke UG (2017) Plant xylem hydraulics: what we understand, current research, and future challenges. *J Integr Plant Biol* 59(6):356–389
- Miller CT, Bruning K, Talbot CL, McClure JE, Gray WG (2019) Nonhysteretic capillary pressure in two-fluid porous medium systems: definition, evaluation, validation, and dynamics. *Water Resour Res* 55(8):6825–6849
- Hassanizadeh SM, Gray WG (1993) Thermodynamic basis of capillary pressure in porous media. *Water Resour Res* 29(10):3389–3405
- Bear J, Bachmat Y (1991) Introduction to modeling of transport phenomena in porous media. Kluwer Academic Publisher, Netherlands
- Starnoni M, Pokrajac D (2020) On the concept of macroscopic capillary pressure in two-phase porous media flow. *Adv Water Resour* 135:103487
- Li Y, Liu C, Li H, Chen S, Lu K, Zhang Q, Luo H (2022) A review on measurement of the dynamic effect in capillary pressure. *J Petrol Sci Eng* 208:109672
- Drelich J, Fang C, White CL (2002) Measurement of interfacial tension in fluid–fluid systems. *Encyclopedia of surface and colloid science* 3:3158–3163
- Hebbar RS, Isloor AM, Ismail AF (2017) Contact angle measurements. In *Membrane characterization* (pp. 219–255). Elsevier
- Alghunaim A, Kirdponpattara S, Newby BMZ (2016) Techniques for determining contact angle and wettability of powders. *Powder Technol* 287:201–215
- Dana D, Saguy IS (2006) Mechanism of oil uptake during deep-fat frying and the surfactant effect-theory and myth. *Adv Coll Interface Sci* 128:267–272
- Alam T, Takhar PS (2016) Microstructural characterization of fried potato disks using X-ray micro computed tomography. *J Food Sci* 81(3):E651–E664
- Reeve RM, Neel EM (1960) Microscopic structure of potato chips. *Am Potato J* 37(2):45–52
- Spiruta SL, Mackey A (1961) French-fried potatoes: palatability as related to microscopic structure of frozen par-fries. *J Food Sci* 26(6):656–662
- Harimi B, Ghazanfari MH, Masihi M (2020) Modeling of capillary pressure in horizontal rough-walled fractures in the presence of liquid bridges. *J Petrol Sci Eng* 185:106642
- Maqsood A, Bussi ere B, Aubertin M, Mbonimpa M (2012) Predicting hysteresis of the water retention curve from basic properties of granular soils. *Geotech Geol Eng* 30(5):1147–1159
- Likos WJ, Lu N, Godt JW (2014) Hysteresis and uncertainty in soil water-retention curve parameters. *J Geotech Geoenviron Eng* 140(4):04013050
- Abbasi F, Javaux M, Vanclooster M, Feyen J (2012) Estimating hysteresis in the soil water retention curve from monolith experiments. *Geoderma* 189:480–490

39. Nuth M, Laloui L (2008) Advances in modelling hysteretic water retention curve in deformable soils. *Comput Geotech* 35(6):835–844
40. Pedroso DM, Williams DJ (2010) A novel approach for modelling soil–water characteristic curves with hysteresis. *Comput Geotech* 37(3):374–380
41. Šimůnek J, Kodešová R, Gribb MM, van Genuchten MT (1999) Estimating hysteresis in the soil water retention function from cone permeameter experiments. *Water Resour Res* 35(5):1329–1345
42. Yakhshi-Tafti E, Kumar R, Cho HJ (2011) Measurement of surface interfacial tension as a function of temperature using pendant drop images. *Int J Optomechatronics* 5(4):393–403
43. Grant SA, Salehzadeh A (1996) Calculation of temperature effects on wetting coefficients of porous solids and their capillary pressure functions. *Water Resour Res* 32(2):261–270
44. Kang W, Chung WY (2009) Liquid water diffusivity of wood from the capillary pressure–moisture relation. *J Wood Sci* 55(2):91–99
45. Spolek GA, Plumb OA (1981) Capillary pressure in softwoods. *Wood Sci Technol* 15(3):189–199
46. Philip JR, De Vries DA (1957) Moisture movement in porous materials under temperature gradients. *EOS Trans Am Geophys Union* 38(2):222–232
47. Nimmo JR, Miller EE (1986) The temperature dependence of isothermal moisture vs. potential characteristics of soils. *Soil Sci Soc Am J* 50(5):1105–1113
48. Van Genuchten MT (1980) A closed-form equation for predicting the hydraulic conductivity of unsaturated soils. *Soil Sci Soc Am J* 44(5):892–898
49. Chen J, Hopmans JW, Grismer ME (1999) Parameter estimation of two-fluid capillary pressure–saturation and permeability functions. *Adv Water Resour* 22(5):479–493
50. Yang X, You X (2013) Estimating parameters of van Genuchten model for soil water retention curve by intelligent algorithms. *Applied Mathematics & Information Sciences* 7(5):1977
51. Li B, Tchelepi HA, Benson SM (2013) Influence of capillary-pressure models on CO<sub>2</sub> solubility trapping. *Adv Water Resour* 62:488–498
52. Webb SW (2000) A simple extension of two-phase characteristic curves to include the dry region. *Water Resour Res* 36(6):1425–1430
53. Troygot O, Saguy IS, Wallach R (2011) Modeling rehydration of porous food materials: I. Determination of characteristic curve from water sorption isotherms. *J Food Eng* 105(3):408–415
54. Alonso EE, Pereira JM, Vaunat J, Olivella S (2010) A microstructurally based effective stress for unsaturated soils. *Géotechnique* 60(12):913–925
55. Mualem Y (1976) A new model for predicting the hydraulic conductivity of unsaturated porous media. *Water Resour Res* 12(3):513–522
56. Burdine N (1953) Relative permeability calculations from pore size distribution data. *J Petrol Technol* 5(03):71–78
57. Brooks RH, Corey AT (1964) Hydraulic properties of porous media and their relation to drainage design. *Transactions of the ASAE* 7(1):26–0028
58. Ippisch O, Vogel HJ, Bastian P (2006) Validity limits for the van Genuchten–Mualem model and implications for parameter estimation and numerical simulation. *Adv Water Resour* 29(12):1780–1789
59. Durner W (1994) Hydraulic conductivity estimation for soils with heterogeneous pore structure. *Water Resour Res* 30(2):211–223
60. Rogers C, Stallybrass MP, Clements DL (1983) On two phase filtration under gravity and with boundary infiltration: application of a Bäcklund transformation. *Nonlinear Anal Theory Methods Appl* 7(7):785–799
61. Russo D (1988) Determining soil hydraulic properties by parameter estimation: on the selection of a model for the hydraulic properties. *Water Resour Res* 24(3):453–459
62. Silin D, Patzek T, Benson SM (2009) A model of buoyancy-driven two-phase countercurrent fluid flow. *Transp Porous Media* 76(3):449–469
63. Grant SA, Bachmann J (2002) Effect of temperature on capillary pressure. *Geophys Monogr–Am Geophys Union* 129:199–212
64. Gaines GL Jr (1972) Surface and interfacial tension of polymer liquids—a review. *Polym Eng Sci* 12(1):1–11
65. Jasper JJ (1972) The surface tension of pure liquid compounds. *J Phys Chem Ref Data* 1(4):841–1010
66. Grant SA (2003) Extension of a temperature effects model for capillary pressure saturation relations. *Water Resour Res* 39(1), SBH-1
67. She HY, Sleep BE (1998) The effect of temperature on capillary pressure–saturation relationships for air–water and perchloroethylene–water systems. *Water Resour Res* 34(10):2587–2597
68. McPhee C, Reed J, Zubizarreta I (2015) Capillary pressure. In *Developments in Petroleum Science* (Vol. 64, pp. 449–517). Elsevier
69. Halder A, Datta AK, Spanswick RM (2011) Water transport in cellular tissues during thermal processing. *AIChe J* 57(9):2574–2588
70. Stevenson CD, Dykstra MJ, Lanier TC (2013) Capillary pressure as related to water holding in polyacrylamide and chicken protein gels. *J Food Sci* 78(2):C145–C151
71. Hamraoui A, Nylander T (2002) Analytical approach for the Lucas–Washburn equation. *J Colloid Interface Sci* 250(2):415–421
72. Cai J, Jin T, Kou J, Zou S, Xiao J, Meng Q (2021) Lucas–Washburn equation-based modeling of capillary-driven flow in porous systems. *Langmuir* 37(5):1623–1636
73. Carbonell S, Hey MJ, Mitchell JR, Roberts CJ, Hipkiss J, Vercauteren J (2004) Capillary flow and rheology measurements on chocolate crumb/sunflower oil mixtures. *J Food Sci* 69(9):E465–E470
74. Saguy IS, Marabi A, Wallach R (2005) New approach to model rehydration of dry food particulates utilizing principles of liquid transport in porous media. *Trends Food Sci Technol* 16(11):495–506
75. Kalogianni EP, Papastergiadis E (2014) Crust pore characteristics and their development during frying of French-fries. *J Food Eng* 120:175–182
76. Saguy IS, Marabi A, Wallach R (2005) Liquid imbibition during rehydration of dry porous foods. *Innov Food Sci Emerg Technol* 6(1):37–43
77. Lisgarten ND, Sambles JR, Skinner LM (1971) Vapour pressure over curved surfaces—the Kelvin equation. *Contemp Phys* 12(6):575–593
78. Dhall A, Datta AK (2011) Transport in deformable food materials: a poromechanics approach. *Chem Eng Sci* 66(24):6482–6497
79. Billings SW, Bronlund JE, Paterson AHJ (2006) Effects of capillary condensation on the caking of bulk sucrose. *J Food Eng* 77(4):887–895
80. Rosa GS, Moraes MA, Pinto LA (2010) Moisture sorption properties of chitosan. *LWT–Food Sci Technol* 43(3):415–420
81. Labuza TP, Rutman M (1968) The effect of surface active agents on sorption isotherms of a model food system. *Can J Chem Eng* 46(5):364–368
82. Al-Rub FAA, Datta R (1998) Theoretical study of vapor pressure of pure liquids in porous media. *Fluid Phase Equilib* 147(1–2):65–83
83. Fisher LR, Israelachvili JN (1979) Direct experimental verification of the Kelvin equation for capillary condensation. *Nature* 277(5697):548–549
84. Haynes JM (1973) Pore size analysis according to the Kelvin equation. *Matériaux et Construction* 6(3):209–213
85. Svintradze DV (2020) Generalization of the Kelvin equation for arbitrarily curved surfaces. *Phys Lett A* 384(20):126412

86. Wang Y, Shardt N, Lu C, Li H, Elliott JA, Jin Z (2020) Validity of the Kelvin equation and the equation-of-state-with-capillary-pressure model for the phase behavior of a pure component under nanoconfinement. *Chem Eng Sci* 226:115839
87. Shereshefsky JL (1928) A study of vapor pressures in small capillaries. Part I. Water vapor.(A). *Soft glass capillaries* 1, 2. *J Am Chem Soc* 50(11):2966–2980
88. Shereshefsky JL, Carter CP (1950) Liquid—vapor equilibrium in microscopic capillaries. I I. Aqueous system. *J Am Chem Soc* 72(8):3682–3686
89. Folman M, Shereshefsky JL (1955) Liquid-vapor equilibrium in microscopic capillaries. I. Non-aqueous Systems. *J Phys Chem* 59(7):607–610
90. Coleburn NL, Shereshefsky JL (1972) Liquid-vapor equilibrium in microscopic capillaries. III. Toluene. *J Colloid Interface Sci* 38(1):84–90
91. McGavack J Jr, Patrick WA (1920) The adsorption of sulfur dioxide by the gel of silicic acid. *J Am Chem Soc* 42(5):946–978
92. Everett DH, Whitton WI (1955) A thermodynamic study of the adsorption of benzene vapour by active charcoals. *Proceedings of the Royal Society of London. Series A. Mathematical and Physical Sciences* 230(1180):91–110
93. Pierce C, Wiley JW, Smith RN (1949) Capillarity and surface area of charcoal. *J Phys Chem* 53(5):669–683
94. Jaros M, Cenkowski S, Jayas DS, Pabis S (1992) A method of determination of the diffusion coefficient based on kernel moisture content and its temperature. *Drying Technol* 10(1):213–222
95. Kang S, Delwiche SR (1999) Moisture diffusion modeling of wheat kernels during soaking. *Transactions of the ASAE* 42(5):1359
96. Shivhare US, Raghavan GSV, Bosisio RG (1994) Modelling the drying kinetics of maize in a microwave environment. *J Agric Eng Res* 57(3):199–205
97. Suarez C, Viollaz P, Chirife J (1980) Diffusional analysis of air drying of grain sorghum. *Int J Food Sci Technol* 15(5):523–531
98. Crank J (1975) Diffusion in a sphere. *The mathematics of diffusion*
99. Datta AK (2007b) Porous media approaches to studying simultaneous heat and mass transfer in food processes. II: property data and representative results. *J Food Eng* 80(1):96–110
100. Halder A, Dhall A, Datta AK (2007a) An improved, easily implementable, porous media based model for deep-fat frying: part I: model development and input parameters. *Food Bioprod Process* 85(3):209–219
101. Ni H, Datta AK (1999) Moisture, oil and energy transport during deep-fat frying of food materials. *Food Bioprod Process* 77(3):194–204
102. Ni H, Datta AK, Torrance KE (1999) Moisture transport in intensive microwave heating of biomaterials: a multiphase porous media model. *Int J Heat Mass Transf* 42(8):1501–1512
103. Halder A, Dhall A, Datta AK (2007b) An improved, easily implementable, porous media based model for deep-fat frying: part II: results, validation and sensitivity analysis. *Food Bioprod Process* 85(3):220–230
104. Gulati T, Zhu H, Datta AK (2016) Coupled electromagnetics, multiphase transport and large deformation model for microwave drying. *Chem Eng Sci* 156:206–228
105. Warning A, Dhall A, Mitrea D, Datta AK (2012) Porous media based model for deep-fat vacuum frying potato chips. *J Food Eng* 110(3):428–440
106. Rakesh V, Datta AK, Walton JH, McCarthy KL, McCarthy MJ (2012) Microwave combination heating: coupled electromagnetics-multiphase porous media modeling and MRI experimentation. *AIChE J* 58(4):1262–1278
107. Ni H (1997) Multiphase moisture transport in porous media under intensive microwave heating. Cornell University
108. Takhar PS (2011) Hybrid mixture theory based moisture transport and stress development in corn kernels during drying: coupled fluid transport and stress equations. *J Food Eng* 105(4):663–670
109. Takhar PS, Maier DE, Campanella OH, Chen G (2011) Hybrid mixture theory based moisture transport and stress development in corn kernels during drying: validation and simulation results. *J Food Eng* 106(4):275–282
110. Takhar PS (2014) Unsaturated fluid transport in swelling poroviscoelastic biopolymers. *Chem Eng Sci* 109:98–110
111. Bansal HS, Takhar PS, Alvarado CZ, Thompson LD (2015) Transport mechanisms and quality changes during frying of chicken nuggets—hybrid mixture theory based modeling and experimental verification. *J Food Sci* 80(12):E2759–E2773
112. Sandhu JS, Takhar PS (2018) Verification of hybrid mixture theory based two-scale unsaturated transport processes using controlled frying experiments. *Food Bioprod Process* 110:26–39
113. Ozturk OK, Takhar PS (2020) Hybrid mixture theory-based modeling of moisture transport coupled with quality changes in strawberries and carrots. *Drying Technol* 39(7):932–949
114. Collman BD, Noll W (1963) The thermodynamics of elastic materials with heat conduction. *Arch Ration Mech Anal* 13:167
115. Sansano M, De los Reyes, R., Andrés, A., & Heredia, A. (2018) Effect of microwave frying on acrylamide generation, mass transfer, color, and texture in french fries. *Food Bioprocess Technol* 11(10):1934–1939
116. Sansano M, Juan-Borrás M, Escriche I, Andrés A, Heredia A (2015) Effect of pretreatments and air-frying, a novel technology, on acrylamide generation in fried potatoes. *J Food Sci* 80(5):T1120–T1128
117. Sandhu J, Bansal H, Takhar PS (2013) Experimental measurement of physical pressure in foods during frying. *J Food Eng* 115(2):272–277
118. Parikh A, Takhar PS (2016) Comparison of microwave and conventional frying on quality attributes and fat content of potatoes. *J Food Sci* 81(11):E2743–E2755

**Publisher's Note** Springer Nature remains neutral with regard to jurisdictional claims in published maps and institutional affiliations.

Springer Nature or its licensor (e.g. a society or other partner) holds exclusive rights to this article under a publishing agreement with the author(s) or other rightsholder(s); author self-archiving of the accepted manuscript version of this article is solely governed by the terms of such publishing agreement and applicable law.